2003

Remote power delivery and signal amplification for MEMS applications

Sunitha Kopparthi
Louisiana State University and Agricultural and Mechanical College

REMOTE POWER DELIVERY AND SIGNAL AMPLIFICATION FOR MEMS APPLICATIONS

A Thesis
Submitted to the Graduate Faculty of the
Louisiana State University and
Agricultural and Mechanical College
in partial fulfillment of the
requirements for the degree of
Master in Science in electrical engineering

in

The Department of Electrical and Computer Engineering

by
Sunitha Kopparthi
B.E., Andhra University, India, 2000
December 2003

Dedicated to my parents, sister and husband

ACKNOWLEDGEMENTS

I would like, first, to express my deepest appreciation for the technical guidance and support given by research advisor, Professor Pratul K. Ajmera.

I would like to thank Dr. Ashok Srivastava and Dr. Martin Feldman for being a part of my thesis committee.

I want to dedicate this work to my parents and sister for their constant encouragement and support throughout my life and to my husband for his advice and emotional support whenever needed.

I would like to express my gratitude to Steve Schmeckpeper, James Breedlove and Golden Hwuang for helping me in experimental setup.

I would also like to thank my friends for their support, cooperation and companionship during my stay at LSU.

I gratefully acknowledge partial support of this work by National Science Foundation and Louisiana Board of Regents through EPSCoR program under Grant No. 0092001. I would like to thank Electrical and Computer Engineering department for providing partial support through teaching assistantship.

TABLE OF CONTENTS

LIST OF TABLES

LIST OF FIGURES

ABSTRACT

Device such as remotely located sensors and bio-implanted devices such as gastric pacer require power for operation. The most commonly used energy source for such devices is a battery cell included in the receiver capsule. Wires can also be used with an external power source but in some applications have serious limitations. This work examines a wireless power transmitter and receiver system to provide power to a remotely located microsystem. Inductive power coupling is the method of choice.

For gastric pacer application, external transmitter coil can be worn around the waist as a belt and the receiver coil can be a part of a remotely located bio-implanted system. The coupling between transmitter and receiver coils when the diameters are markedly different is analyzed. A conventional rectifier circuit converts ac voltage to required dc voltage. This dc voltage supplies power to the charging chip, which is used to recharge lithium batteries in the implanted system. For an input supply voltage of 0.35 V_{rms}, the induced voltage in the receiver coil across the load resistor was 0.37 V_{rms}, when the receiver coil was placed at the center of the transmitter coil. When the receiver coil was placed close to the rim of the transmitter, the induced voltage across the load resistor for the same input supply voltage was 0.67 V_{rms}. Corresponding transmitted power to the load resistor of the receiver coil were 4 and 13.2 mW, respectively. Means are suggested to improve the power transfer to the receiver coil.

The second objective of this thesis is to design an op-amp for on-chip amplification of sensor signals. On-chip detection and amplification are crucial for obtaining high sensitivity and improved signal to noise ratio. Designed op-amp is simulated using PSPICE with Level-3 MOS model parameters. The simulation results show a gain of 40.7 dB and a 3-dB bandwidth of 580 kHz. Experimental measurements made on the fabricated chip observed a gain of 3 and a 3-dB

bandwidth of 1 MHz, which was attributed to differences in the values of simulated model parameters and the values appropriate for the fabrication process used by the foundry.

1. INTRODUCTION

1.1 Background

There are a variety of situations in which electrical energy is needed at a remote inaccessible region such as a site within a body or in a toxic or hazardous environment. Advanced treatments for a variety of diseases are likely to require electrical energy for powering bio-implanted units within a body. The electrical energy can be supplied to a bio-implanted site by means of an implanted battery, or by wires penetrating through skin or by a wireless technique. The former requires periodic surgery to replace the battery. The latter requires patient to be near the wireless transmitter. There is another option that is considered in this work. Here, a rechargeable battery is implanted and is charged periodically by a wireless transmitter. Inductive coupling between a coil, external to the body and a receiving coil, implanted within the body is the mechanism used in this work for remote power transfer. The use of inductive coupling of power for battery charging eliminates the need for surgery for battery replacement, and improves quality of life of the patient.

Another option is for the implanted microcircuits or devices to be energized directly by an electromagnetic field. The advantage to this method is that a local power source such as a battery can now be completely avoided, eliminating the risk of leakage of poisonous battery substances into the body. The disadvantage is that the patient must be near an external transmitter at all times. The energy transfer by electromagnetic coupling between inductor coils can be carried out in bioengineering and other applications, if attention is paid to important matters such as frequency, losses in the intermediary medium, coil configuration and other geometrical parameters. In this work, a system is designed for remote delivery of power by

means of coupled coils to supply power to a bio-implanted rechargeable battery or to a remotely located device.

1.2 Literature Review

Heetderks [1] examined the feasibility of designing millimeter and submillimeter-sized transducers based on radio frequency (RF) coupling that could be integrated into new implants to provide power to transducers for neural stimulation without a tethering power cable. He also analyzed special cases of transformer coupling between millimeter-sized or submillimeter-sized receiver coils to large centimeter- and decimeter-sized transmitter coils.

Radio frequency has been investigated as a source of external power for miniature and long-term implant telemetry systems. Ko et al. [2] designed RF powered coils for implant instruments in which power transfer from the transmitter coil to the receiver coil was achieved at a frequency of 3.5 MHz. The RF power output from an oscillator is amplified and is used to drive a transmitting coil. The receiver picks up the transmitted RF power, and a power receiving circuit rectifies the induced RF and converts into a regulated dc supply for the implanted electronic system.

Schuder et al. [3] designed an inductively coupled RF system that can transmit 1 kW of power through the skin to anticipate energy requirements for a patient with an artificial heart. The inductive coupling between a pancake-shaped coil on the surface of the body and a similar coil within the body was utilized for the transportation of the electromagnetic energy. The temperature rise in the tissue is intimately related to reduction of losses in the region of the implanted coil.

Ziaie et al. [4] developed a single-channel implantable microstimulator for functional neuromuscular stimulation. This device $2 \times 2 \times 10$ mm^3 in dimension can be inserted into paralyzed muscle groups by a hypodermic needle. The microstimulator is powered and

controlled through an inductive telemetry link driven by a class E power amplifier at a frequency of 2 MHz.

Smith et al. [5] developed an implantable muscle stimulator using semi-custom integrated circuit technology for versatile control of paralyzed muscles. The stimulator circuit is externally controlled and powered by a single encoded RF carrier at 10 MHz. Up to eight independently controlled stimulus output channels are provided with output channel selection, stimulus pulse width, and stimulus pulse frequency under external control.

Radio frequency coils are used extensively in the design of implantable devices for transdermal power and data transmission. Soma et al. [6] presented a theoretical analysis of misalignment effects such as lateral and angular misalignment in RF coil systems. A design procedure is established to maximize coil coupling for a given configuration.

Flack et al. [7] computed the value of mutual inductance between two circular conductors lying in parallel planes for a variety of plane spacings and displacements between the coils axes.

Hochmair [8] designed a transcutaneous signal transmission system for an auditory prosthesis. By employing "critical coupling" between the implanted and external circuits, a stable transcutaneous transmission of power and signal via two coupled coils with a minimized dependence on the relative spacing of the coils was achieved. Optimizing coil geometries and preventing saturation of the RF output amplifier was found necessary to approximately maintain critical coupling despite placement tolerances within a reasonable range.

Wu et al. [9] demonstrated a simple wireless powering scheme, which utilizes a transformer with an air gap in its core. The transformer secondary is fabricated on-chip and is detachable from the transformer. Transformer operates at frequencies less than a few MHz and is capable of handling high voltage (223.4 V_{pp}) and high power delivery to the load (4.5 W_{rms}).

An improvement in the efficiency of energy transport in a system involving inductive coupling between an external and an internal coil is realized when a suitable ferrite core is utilized for the implanted coil [10]. For a system with a low initial value of efficiency, the insertion of a suitable core results in a several-fold improvement in energy transport efficiency. In general, however the increase in efficiency can be more easily realized by an increase in the radius of the receiving coil.

Schuylenbergh and Puers [11] showed that an inductively coupled powering system is fully compatible with a hospital environment. Moreover, the results can be expanded to other remote powering applications characterized by difficult coil coupling conditions, such as miniature implanted stimulators and telemetry in artificial knee or hip joints.

Puers et al. [12] described a system for detecting loosening of hip prosthesis based on a mechanical vibration method. The system consists of a circuit that is embedded in a cavity inside the prosthesis. It uses two wireless links. The circuit detects the vibration and converts it to electrical signal. One of the links is used to power the implantable circuit and the second one transmits the electronic signal from the implant to a personal computer, using a data acquisition card.

Donaldson, and Perkins [13] developed theory of coupled resonant coils for design of RF transcutaneous links having simultaneously a high overall efficiency and good displacement tolerance while keeping the circuitry simple. For high efficiency, series tuned transmitter coils are used. Two examples were described; the first stimulator design had excellent displacement tolerance when operated at critical coupling frequency and the second example dealt with the involved theory when voltage is regulated to supply internal power to the implants.

As described in section 1.3 below, a part of this thesis deals with on-chip amplification of sensor signal in MEMS amplification. Gray and Meyer [14] have presented an overview of

current design techniques for operational amplifier implementation in CMOS and NMOS technology at a tutorial level with primary emphasis on CMOS amplifiers.

1.3 Research Objectives and Scope

Looking at the available literature, there is little work reported on coupling between transmitter and receiver coils, when the coil diameters are distinctly different and located relatively far away from each other and the received power is approximately half a watt. In a reported work related to coupling between transmitter and receiver coils with the coils having almost the same diameter placed close to each other about 1.5 cm [3], high power transfer of about 1 kW has been achieved. However, in another reported work, coils with different diameters placed far apart achieved power coupling of less than 1 mW [1].

One of the main aims of this research is to develop a coupled coil system for remote transmission of power. Though this approach is general in nature, it is applied here to a specific application. This application is remote power transmission for a bio-implanted gastric pacer. Here, the transmitter coil is worn around the waist and the receiver coil is implanted inside the body near the stomach wall. The remotely transmitted and received power will be used to charge rechargeable batteries located inside the implanted device. The receiver coil, rechargeable batteries and the stimulator circuitry are to be implanted in the body. It is important that their collective size is small. The transmitter circuit should be designed in such a way that it is easy to use and does not hamper the patient's daily routine significantly. These requirements for the system impose constraints to the design of the inductive link. An optimal coil set is designed after taking into consideration the internal power needs, the available space and patient comfort.

An analysis for the coupling between a transmitter coil and receiver coil when the coil diameters are different is carried out. The voltage signal appearing across the receiver coil is rectified by a full wave rectifier which is connected to a load resistor. For high system efficiency,

maximization of power transfer from the transmitting coil to the receiving coil is desired. A design procedure for the transmitting and receiving coils has been established based on voltage and power requirement at the receiver load.

Integration of microelectromechanical (MEM) structures with electronic circuitry on the same chip has been of significant interest in recent years as it has distinct advantages in size, sensitivity, reliability and fabrication cost.

The second objective of this thesis is to design an amplifier for on-chip amplification of sensor signals. On-chip amplification for a variety of microsystem applications is desired when the sensor signals are small and/or are present in a noisy environment.

1.4 Organization of Thesis

Chapter 2 provides the necessary background for designing a system for wireless power transmission. Chapter 3 provides design considerations and the design of the transmitter and receiver coils. Chapter 4 presents description of the model and results for the wireless power transmission between the transmitter and receiver coils. Chapter 5 gives the design of an operational amplifier for on-chip amplification of sensor signals. Chapter 6 summarizes the results, discusses its limitations and gives recommendations for future work.

2. BACKGROUND THEORY FOR COIL DESIGN

It is desirable for implantable microsystems to have no interconnect leads. Therefore, wireless inductive powering is an attractive solution based on magnetic coupling between the transmitter coil external to the body and the receiver coil implanted in the body. Before going into the details of coil design, some of the basic concepts are reviewed in this chapter.

2.1 Linear Passive Reactive Circuit Elements

2.1.1 Capacitance

Capacitor is a linear circuit element that is capable of storing energy in its electric field. It consists of two conducting surfaces separated by a non-conducting, or dielectric material. The charge difference between the plates creates an electric field that stores the energy. Because of presence of the dielectric, the conduction current that flows in the wires that connect to capacitor cannot flow internally between the plates. When an electric field or voltage varies with time there exists conduction current, equal to displacement current that flows between the plates of the conductor. Capacitance C in farads is a measure of capacitor's ability to store charge on the plates and is given by

$$C = \frac{Q}{V} \tag{2.1}$$

where Q is charge stored on the capacitor plate in coulombs and V is voltage difference between the two plates in volts. For a parallel plate capacitance

$$C = \frac{\varepsilon A}{d} = \frac{\varepsilon_o \varepsilon_r A}{d} \tag{2.2}$$

where A is the plate area, d is the distance between the plates, ε_r is the relative permittivity of the dielectric and ε_o is permittivity of free space.

There are many different kinds of capacitors, and are categorized by the type of dielectric material that is used between the plates. Although any good insulator can serve as a dielectric, each type has characteristics that make it more suitable for particular applications. For general applications in electronic circuits, the dielectric material may be paper impregnated with oil or other material such as wax, mylar, polystyrene, mica, glass, or ceramic. Ceramic dielectric capacitors constructed of barium titanates have a large capacitance-to-volume ratio because of their high dielectric constant. Mica, glass, and ceramic dielectric capacitors will operate satisfactorily at high frequencies. Aluminum electrolyte capacitors, which consist of a pair of aluminum plates separated by a moistened borax paste electrolyte, can provide high values of capacitance in small volumes. They are typically used as by-pass and coupling capacitors and in filters, power supplies and as starting capacitor in motors. Tantalum electrolyte capacitors have lower losses and have more stable characteristic than those of aluminum electrolyte capacitors. Energy $W_C(t)$ stored in a capacitor is given by

$$W_C(t) = \frac{1}{2} C v^2(t) \tag{2.3}$$

where v(t) is voltage difference between the capacitor plates.

2.1.2 Inductor

Inductor is a linear element that is capable of storing energy in its magnetic field. If a coil of N turns is connected to a voltage v to drive current i through the coil, it generates magnetic flux ϕ as determined by Faraday's law:

$$v = N \frac{d\phi}{dt} \quad \text{(volts)} \tag{2.4}$$

where N represents the number of turns of the coil and $d\phi/dt$ is the instantaneous change in flux ϕ linking the coil. If the current increases in magnitude, the flux linking the coil also increases.

Changing the flux linked with coil, induces voltage across the coil. The polarity of this induced voltage tends to establish a current in the coil, which produces a flux that will oppose any change in the original flux. The instant the current begins to increase in magnitude, the opposing effect tends to limit the change. The change in current through the coil is termed as "choking". General principle of this effect is known as Lenz's law, which states that induced effect is always such as to oppose the cause that produces it. The ability of a coil to oppose any change in current is a measure of the self-inductance or inductance L of the coil. Inductance of a coil is also a measure of change in flux ϕ linking a coil due to change in current *i* through the coil and is given by

$$L = N\frac{d\phi}{di}. \tag{2.5}$$

Substituting Eq. 2.5 in Eq. 2.4, we have

$$v = N\frac{d\phi}{dt} = \left(N\frac{d\phi}{di}\right)\left(\frac{di}{dt}\right) = L\frac{di}{dt}. \tag{2.6}$$

The number of flux lines per unit area is called the flux density, denoted by the capital letter B.

If cores of different materials with the same physical dimensions are used in an electromagnet, the strength of the magnet will vary in accordance with the core used. This variation in strength is due to greater or lesser number of flux lines passing through the core. Materials in which flux lines can be readily set up have high permeability μ, which is a measure of the ease with which magnetic flux lines can be established in the material. The permeability of non-magnetic materials, such as copper, aluminum, wood, glass, and air, is approximately the same as that for the free space value μ_o. Materials that have permeabilities less than μ_o are diamagnetic, and those with permeabilities greater than μ_o are paramagnetic. Ferromagnetic materials, such as iron, nickel, steel, cobalt, and alloys of these metals, have permeabilities hundreds and even thousands of times that of free space. The reluctance R_{rel} of a material to the

setting up of magnetic flux lines is given by

$$R_{rel} = \frac{l_m}{\mu A} \qquad \text{[rels]} \tag{2.7}$$

where l_m is length of the magnetic path, and A is its cross-sectional area. For magnetic circuits, flux ϕ is given by

$$\phi = \frac{\mathrm{M_F}}{\mathrm{R}} \tag{2.8}$$

where M_F is the magnetomotive force and is proportional to the product of the number of turns N around the core (in which the flux is to be established) and the current *i* through the turns or

$$\mathrm{M_F} = \mathrm{N\,i}\,. \tag{2.9}$$

Magnetizing force (H) is magnetomotive force per unit length

$$H = \frac{\mathrm{M_F}}{l_m} = \frac{N\,i}{l_m}\,. \tag{2.10}$$

Hence, inductance L is given by

$$L = N\frac{d\phi}{di} = N\frac{d(\mathrm{M_F}/R)}{di} = N\frac{d(Ni\mu A/l_m)}{di} = \frac{N^2\mu A}{l_m} = \frac{N^2\mu_r\mu_o A}{l_m} \tag{2.11}$$

where μ_r is relative permeability of the core material.

Associated with every inductor are a resistance equal to the resistance R_l of the turns and a parasitic capacitance between the turns of the coil. To include these effects, an approximate lumped equivalent model for an inductor is shown in Fig. 2.1. For some applications, the parasitic capacitance appearing in the Fig. 2.1 can be ignored, resulting in a simplified equivalent model of Fig. 2.2. Energy $W_L(t)$ stored in the magnetic field by an inductor L carrying current i(t) is given by

$$W_L(t) = \frac{1}{2}Li(t)^2\,. \tag{2.12}$$

Inductors are categorized by the type of the core on which they are wound as shown in Fig. 2.3. For example, the core material may be air or any non-magnetic material, or magnetic material such as iron, or ferrite as shown in Fig. 2.3. Inductors made with air or nonmagnetic materials are widely used in radio, television, and filter circuits. Iron-core inductors are used in electrical power supplies and filters. Ferrite-core inductors are widely used in high-frequency applications. The permeability-tuned variable coil has a ferromagnetic shaft that can be moved within the coil to vary the flux linkages of the coil and thereby its inductance.

2.2 Resonance

Resonant circuit is a combination of R, L, and C elements. For a particular frequency when the reactive component of the impedance is equal to zero then the circuit is said to be in resonance. The frequency at which resonance occurs is called the resonance frequency. Inductor has parasitic capacitance C_{par} as shown in the Fig. 2.1. For a particular frequency when the reactance of the parasitic capacitance and the inductor are equal in magnitude, the inductor is said to be in resonance and this particular phenomenon is called self-resonance. At resonance, the energy stored by one reactive element in a part of a cycle is the same as that released by the other reactive element in effect canceling the reactive component of impedance. There are two types of resonant circuits, series and parallel. At resonance, the voltage and current are in phase and the power factor is unity. In the series case, at resonance the impedance is minimum and, the current is maximum for a given voltage. Resonance angular frequency ω_o for a simple RLC circuit is given by

$$\omega_O = \frac{1}{\sqrt{LC}}. \tag{2.13}$$

For a series circuit, the quality factor Q defined as 2π times maximum energy stored at resonance divided by energy lost per cycle is given by

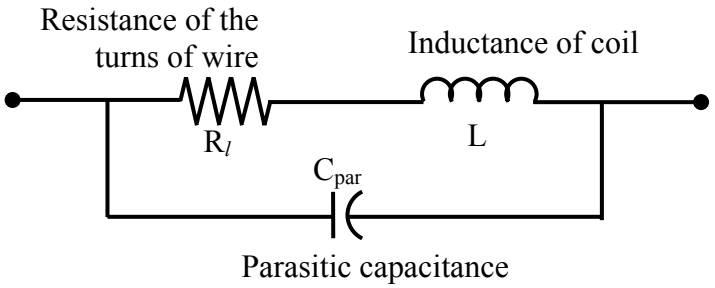

Fig. 2.1: A lumped equivalent model for an inductor.

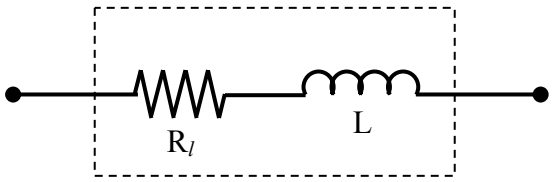

Fig. 2.2: A simplified model for an inductor.

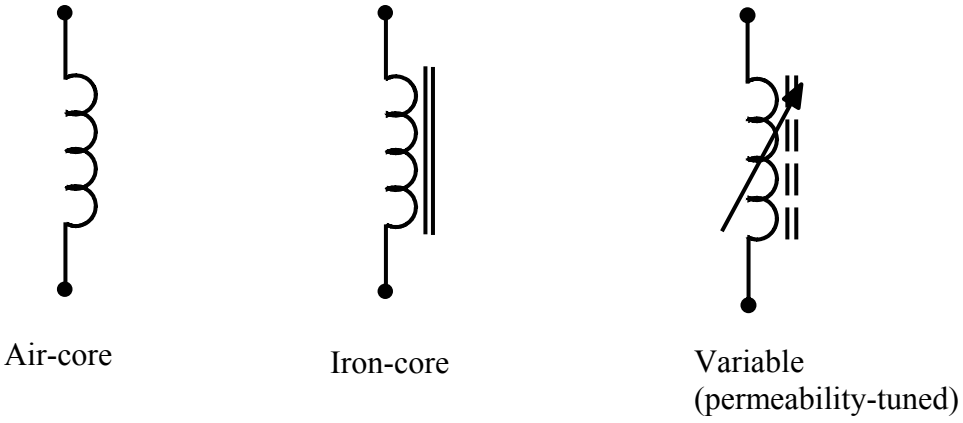

Fig. 2.3: Types of inductors.

$$Q = \frac{\omega_O L}{R} = \frac{1}{\omega_O CR} = \frac{1}{R}\sqrt{\frac{L}{C}}\,. \tag{2.14}$$

The half-power bandwidth BW is given by

$$BW = \frac{\omega_O}{Q}\,. \tag{2.15}$$

The frequency selectivity of the circuit is determined by the value of Q. A high-Q circuit has a small bandwidth and, therefore, the circuit is very selective. A high-Q series circuit has a small value of R, while a high-Q parallel circuit has a relatively large value of R.

2.3 Mutually Coupled Coils

A coil in vacuum or air at low frequency with negligible skin effect has an inductance L given by [15]

$$\mathrm{L} = \mathrm{FN}^2\mathrm{D} \times 10^{-6}\ \mathrm{H} \tag{2.16}$$

where D is the diameter of the coil in inch, N is the number of turns of coil and F is form factor, which is a function of D/*l* ratio where *l* is the length of the coil in inch. Form factor F values are given in reference [15] and are reproduced in the Appendix A on page 66 for convenience. Resistance R of the coil is given by

$$R = \frac{\pi DN}{l_S} \tag{2.17}$$

where l_S is the length per unit resistance of the wire (ft/Ω). The parasitic capacitance C_{par} of the inductor is proportional to the circumference and the number of turns of the coil, and can be approximated as [16]

$$C_{par} = 5.2 \times 10^{-14}\mathrm{DN}, \tag{2.18}$$

where D is the diameter of the coil in inch and capacitance is in F. The weight W of the coil is given by

$$W = \frac{\pi DN}{l_W} \tag{2.19}$$

where l_W is the length per unit weight of the wire (ft/lb) and the self resonance frequency f_{os} of the coil is given by

$$f_{os} = \frac{1}{2\pi\sqrt{LC_{par}}}. \tag{2.20}$$

Consider a case of two coaxial coplanar coils with diameter D_T and D_R and $D_T >> D_R$ with number of turns N_T and N_R respectively in a medium with permeability μ. This corresponds to a small diameter receiver coil being excited by a large diameter transmitter coil. An estimate of the mutual inductance can be obtained from the following analysis. A current I_T through a coil of infinite length produces a magnetic field along the axis H_Z inside the coil given by $H_Z = I_T N'_T$, where N'_T is the number of coil per unit length. For a single turn coil, on the other extreme, magnetic field in the center along the axis is given by

$$H_Z = \frac{I_T {D_T}^2}{8\left(\left(\frac{D_T}{2}\right)^2 + Z^2\right)^{3/2}}, \tag{2.21}$$

where Z is the distance along the normal axis from the center of the loop. At the center of the loop, Z = 0 and $H_Z = I_T / D_T$. If this approach is extended to a thin coil of N_T turns, then in the center of the coil, magnetic field H_Z can be extended by

$$H_Z \approx \frac{I_T N_T}{D_T}. \tag{2.22}$$

The magnetic flux density along the axis normal to the coil is given by

$$B_Z = \frac{I_T N_T \mu}{D_T}. \tag{2.23}$$

If we assume that H is relatively uniform over the small area of the receiver coil, then the flux linkage ϕ_{RT} in the receiver coil due to current I_T in the transmission coil is

$$\phi_{RT} = \left(\frac{N_T I_T \mu}{D_T} \right) \left(\frac{\pi D_R{}^2}{4} \right). \tag{2.24}$$

For the receiver coil, the voltage V_l across the inductor is

$$V_l = -N_R \frac{\partial \phi_{RT}}{\partial t} = -\frac{N_T N_R \pi D_R{}^2 \mu}{4 D_T} \frac{\partial I_T}{\partial t}. \tag{2.25}$$

Mutual inductance M is defined as flux linkage in receiver coil due to unit current in the transmitter coil. From Eq. 2.25, for coaxial coplanar coils M can be given as

$$M = N_R \frac{\partial \phi_{RT}}{\partial I_T} = \frac{\pi}{4} N_T N_R \mu \frac{D_R{}^2}{D_T}. \tag{2.26}$$

Eq. 2.26 can be approximated for the case of a receiver coil that is rectangular, by setting the diameter of the receiver coil such that its cross-sectional area is equal to the rectangular coil. Clearly, larger D_R, smaller D_T, higher N_T and N_R and higher μ are desirable for stronger coupling.

In this chapter, background theory required for the coil design for the remote power transfer has been described. The basic linear reactive elements, inductor and capacitor, are described. Formula for mutual inductance of coaxial coplanar coils is derived.

3. WIRELESS POWER TRANSMISSION

Design of a wireless power transmission and receiver system is discussed in this section. The receiver coil along with other circuitry is bio-implanted in human body or otherwise remotely located. In the application chosen as a demonstration in the current work, rechargeable batteries are implanted with the receiver circuit. The batteries need to be recharged periodically by the designed remote power transmission system. A specific application that of gastric pacing is selected as a vehicle to demonstrate the feasibility of remote power transmission for MEMS. For a gastric pacer, the circuitry for pacing is bio-implanted outside the stomach with electrodes placed at suitable locations. Like a heart pacer, gastric pacing needs continuous pulses. In the current system design, rechargeable Li batteries are implanted with circuitry. A receiver coil is included with the circuitry. A transmitter coil is worn outside the body periodically only during the times necessary to transmit power for recharging the batteries. The primary coil (transmitter) shown in the Fig. 3.1 (a) is a hollow cylinder, which can be worn around the waist as shown in Fig. 3.2. The receiver coil is smaller in size as shown in Fig. 3.1 (b) which is implanted with the circuitry.

3.1 Transmitter Coil Design

The transmitter coil is a hollow cylinder with inner radius of 7.875” and outer radius of 8.175”. This radius was chosen initially to give approximately 50” circumference for a belt to be worn by an obese person. So the radius of the transmitter coil is approximated to 8.025”. The width and the thickness of the transmitter coil were chosen to be 2” and 0.3” respectively. Form factor F is a function of diameter to length (D/*l*) ratio of the coil. The value of the form factor for the transmitter coil F_T is 0.048 as obtained from Fig. A.1 in Appendix A for D/*l* ratio of 8.025.

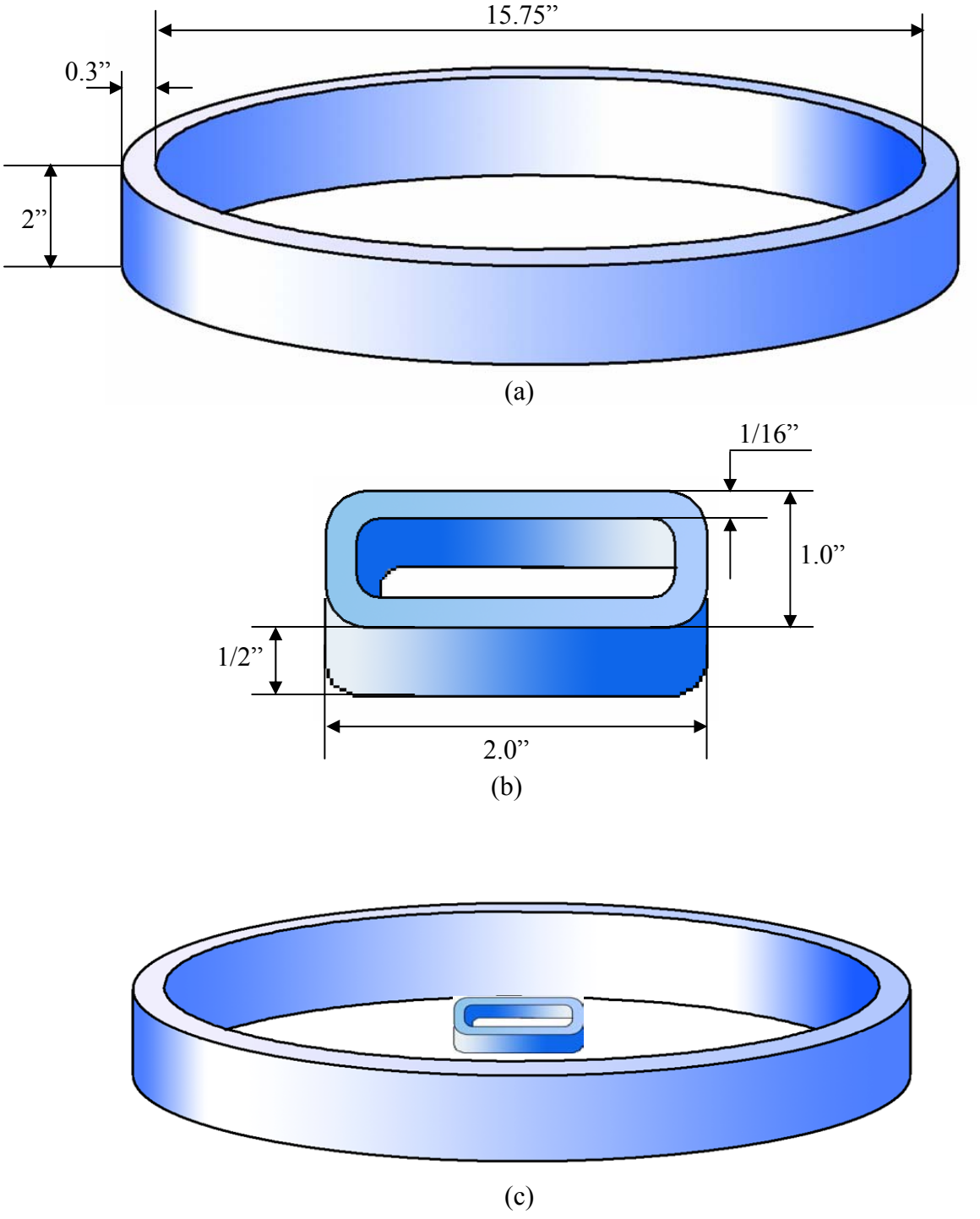

Fig. 3.1: (a) Transmitter or primary coil, (b) Receiver or secondary coil and (c) Wireless power transmission system.

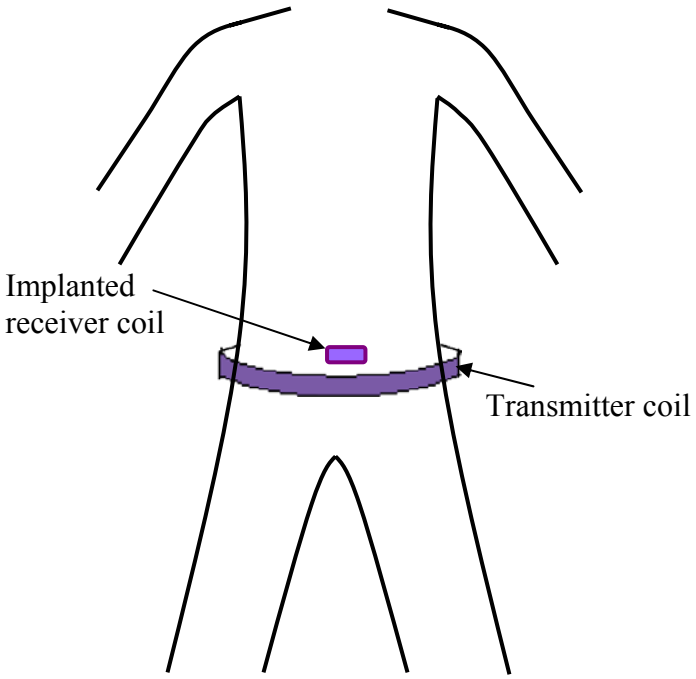

Fig. 3.2: Illustration of complete wireless power transmission system.

The maximum voltage supplied to the transmitter is restricted such that the maximum current through the coil is less than or equal to 0.1 times the fusing current.

- **Turns of the coil:**

For a coil of length l and thickness t, wound with a wire of diameter d, the number of turns along length of the coil in each layer $N_l \approx l$ /d for $l >>$ d and the number of layer N_t that can be fit in thickness t is given by $N_t \approx \frac{t-d}{0.866d} + 1$ as indicated in Fig. 3.3. Total number of turns of the coil $N = N_t \times N_l$. Table A.1 in Appendix A gives the pertinent information on different size standard gauge copper wires. Calculations using a 10 gauge enamel coated copper wire (d = 104.4 mils, l_S = 1001 ft/Ω, and l_W = 31.82 ft/lb) are given below for the transmitter coil design as an example. Similar calculations can be carried out for other wire sizes.

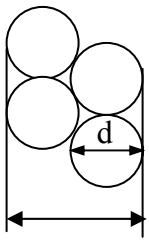

1.866d

Fig. 3.3: Cross-section along thickness of the coil. Diameter of the coil wire is d.

- **Example using 10-gauge enamel coated copper wire:**

Number of turns N_l along 2" length: $N_l \approx$ 2"/104.4 mils = 19.15 ≈ 19.

Number of turns N_t along 0.3" thickness: $N_t \approx (300 - 104.4) / (104.4 \times 0.866) + 1 = 3.16 \approx 3$.

Total turns N_T of transmitter coil: $N_T = N_t \times N_l = 19 \times 3 = 57$.

Resistance of the coil: $R_T \approx \pi D_T N_T / l_S = (3.14 \times 16.05 \times 57) / (1001 \times 12) \approx 0.24\ \Omega$.

Weight of the coil wire: $W_T \approx \pi D_T N_T / l_W = (3.14 \times 16.05 \times 57) / (31.82 \times 12) \approx 7.5$ lb.

Inductance of the coil: Form factor F_T for the transmitter coil ≈ 0.048 from Fig. A.1 in Appendix A for D/*l* ratio of 8.025. $L_T \approx F_T N_T^2 D_T \times 10^{-6}$ H = $0.048 \times (57)^2 \times 16.05 \times 10^{-6}$ = 2.5 mH.

Estimated parasitic capacitance of the coil: From reference [16], $C_{ST} \approx 5.2 \times 10^{-14} D_T N_T = 5.2 \times 10^{-14} \times 16.05 \times 57 \approx 47.6$ pF.

Self-resonance frequency f_{OST} for transmitter coil:

$$f_{OST} = \frac{1}{2\pi}\sqrt{\frac{1}{L_T C_{ST}}} = \frac{1}{2 \times 3.14}\sqrt{\frac{1}{2.5 \times 10^{-3} \times 47.6 \times 10^{-12}}} \approx 462\ kHz.$$

3.2 Receiver Coil Design

The receiver coil for this case will be bio-implanted inside the body for gastric pacing and has to be small in size and weight. The rectangular receiver coil is chosen to improve mutual coupling within the size constraints. The receiver coil parameters, inductance, resistance, parasitic capacitance and the weight of the coil can be calculated using Eqs. 2.16 - 2.19 as done above for the transmitter coil. Here coil diameter is set at a value that results in the same cross-sectional areas as the rectangular coil. Inner and outer effective radii of the receiver coil are 0.64" and 0.7" respectively. Hence the radius of the receiver coil is approximated to be 0.67". The length and thickness of the receiver coil are 0.5" and 0.0625" respectively. The value of the form factor F_R for the receiver coil is 0.032 obtained from Fig. A.1 in Appendix A for D/*l* ratio of 2.68. Calculations using a 20-gauge enamel coated copper wire (d = 33.8 mils, l_S = 98.5 ft/Ω, and l_W = 323.4 ft/lb) are given below for the receiver coil design as an example. Similar calculations can be carried out for other wire diameter sizes.

- **Example using 20-gauge enamel coated copper wire:**

Number of turns N_l along 0.5" length of the coil: N_l = 0.5"/33.8 mils = 14.79 ≈ 15.

Number of turns N_t along 0.0625" thickness of the coil: $N_t = (62.5 - 33.8) / (33.8 \times 0.866) + 1 = 1.98 \approx 2$.

Total turns N_R for the receiver coil: $N_R = N_t \times N_l = 15 \times 2 = 30$.

Resistance R_R of the approximated circular receiver coil: $R_R = \pi D_R N_R / l_S = (3.14 \times 1.34 \times 30) / (98.50 \times 12) = 0.107\ \Omega$.

The actual resistance value of the rectangular receiver coil is $R_R = 2(l_r + w_r)N_R / l_S = 2 \times (1.9375 + 0.9375) \times 30 / (98.50 \times 12) = 0.146\ \Omega$ where l_r and w_r are the effective length and width of the rectangular receiver coil.

Weight W_R of the approximated circular receiver coil wire: $W_R = \pi D_R N_R / l_W = (3.14 \times 1.34 \times 30) / (323.4 \times 12) = 0.033$ lb = 14.97 gm.

Actual weight of the rectangular receiver coil is $W_R = 2(l_r + w_r)N_R / l_W = 2 \times (1.9375 + 0.9375) \times 30 / (323.4 \times 12) = 0.044$ lb = 19.96 gm.

Inductance L_R of the receiver coil: $L_R = F_R N_R^2 D_R \times 10^{-6}$ H $= 0.032 \times (30)^2 \times 1.34 \times 10^{-6} = 38.7 \times 10^{-6} \approx 39\ \mu$H.

Estimated parasitic capacitance C_{SR} of the receiver coil: From reference [16],

$C_{SR} \approx 5.2 \times 10^{-14} D_R N_R = 5.2 \times 10^{-14} \times 1.343 \times 30 \approx 2.1$ pF.

Self-resonance frequency f_{SR} for the receiver coil:

$$f_{SR} = \frac{1}{2\pi}\sqrt{\frac{1}{L_R C_{SR}}} = \frac{1}{2 \times 3.14}\sqrt{\frac{1}{39 \times 10^{-6} \times 2.1 \times 10^{-12}}} \approx 17.6\ MHz.$$

3.3 Design Considerations

For different gauge wires, parameter such as the number of turns, inductance, winding resistance, parasitic capacitance, weight and self resonance of the transmitter and receiver coils were attained as described above and are shown in Table 3.1 and Table 3.2 respectively.

Table 3.1. Transmitter coil parameters for different gauge enameled copper wires. Approximate size of transmitter coil diameter D = 15.75", length l = 2", and thickness t = 0.3".

Wire Gauge	Turns per layer × No. of layers $N_l \times N_t = N_T$	Coil resistance R_T (Ω)	Self inductance L_T (H)	Parasitic capacitance C_{ST} (F)	Self resonance f_{ST} (Hz)
10	19 × 3 = 57	2.39E-01	2.50E-03	4.76E-11	4.62E+05
11	21 × 3 = 63	3.33E-01	3.06E-03	5.27E-11	3.97E+05
12	24 × 4 = 96	6.40E-01	7.10E-03	8.02E-11	2.11E+05
13	27 × 4 = 108	9.08E-01	8.99E-03	9.03E-11	1.77E+05
14	30 × 5 = 150	1.59E+00	1.73E-02	1.25E-10	1.08E+05
15	34 × 5 = 170	2.27E+00	2.23E-02	1.42E-10	8.95E+04
16	38 × 6 = 228	3.85E+00	4.00E-02	1.91E-10	5.76E+04
17	42 × 7 = 294	6.25E+00	6.66E-02	2.46E-10	3.94E+04
18	47 × 7 = 329	8.82E+00	8.34E-02	2.75E-10	3.33E+04
19	53 × 8 = 424	1.43E+01	1.38E-01	3.54E-10	2.27E+04
20	59 × 9 = 531	2.26E+01	2.17E-01	4.44E-10	1.62E+04
21	66 × 10 = 660	3.55E+01	3.36E-01	5.52E-10	1.17E+04
22	74 × 12 = 888	6.02E+01	6.07E-01	7.42E-10	7.50E+03
23	82 × 13 = 1066	9.11E+01	8.75E-01	8.91E-10	5.70E+03
24	92 × 15 = 1380	1.49E+02	1.47E+00	1.15E-09	3.87E+03
25	103 × 16 = 1648	2.24E+02	2.09E+00	1.38E-09	2.97E+03
26	116 × 19 = 2204	3.78E+02	3.74E+00	1.84E-09	1.92E+03
27	129 × 21 = 2709	5.86E+02	5.65E+00	2.26E-09	1.41E+03
28	145 × 23 = 3335	9.09E+02	8.57E+00	2.79E-09	1.03E+03
29	160 × 26 = 4160	1.43E+03	1.33E+01	3.48E-09	7.40E+02
30	180 × 29 = 5220	2.26E+03	2.10E+01	4.36E-09	5.26E+02
31	202 × 32 = 6464	3.53E+03	3.22E+01	5.40E-09	3.82E+02
32	222 × 36 = 7992	5.51E+03	4.92E+01	6.68E-09	2.78E+02
33	250 × 40 = 10000	8.69E+03	7.70E+01	8.36E-09	1.98E+02
34	282 × 45 = 12690	1.39E+04	1.24E+02	1.06E-08	1.39E+02
35	317 × 51 = 16167	2.23E+04	2.01E+02	1.35E-08	9.65E+01
36	351 × 56 = 19656	3.42E+04	2.98E+02	1.64E-08	7.20E+01
37	392 × 63 = 24696	5.42E+04	4.70E+02	2.06E-08	5.11E+01
38	435 × 70 = 30450	8.44E+04	7.14E+02	2.54E-08	3.73E+01
39	500 × 80 = 40000	1.40E+05	1.23E+03	3.34E-08	2.48E+01
40	555 × 89 = 49395	2.18E+05	1.88E+03	4.13E-08	1.81E+01

(Table 3.1 continued)

Wire gauge	Fusing current (A)	Max. current allowed Imax (A)	Pmax, Power Dissipation @ Imax (W)	Imax @ 10 W power dissipation (A)	Vmax @ 10 W power dissipation (V)	Coil weight W_T (lb)
10	333	33.3	2.65E+02	6.47	1.5E+00	7.5
11	280	28	2.61E+02	5.48	1.8E+00	6.6
12	235	23.5	3.54E+02	3.96	2.5E+00	8.0
13	197	19.7	3.53E+02	3.32	3.0E+00	7.1
14	166	16.6	4.38E+02	2.51	4.0E+00	7.8
15	140	14	4.46E+02	2.1	4.8E+00	7.0
16	117	11.7	5.26E+02	1.62	6.2E+00	7.5
17	98.4	9.84	6.05E+02	1.27	7.9E+00	7.7
18	82.9	8.29	6.06E+02	1.07	9.4E+00	6.8
19	69.7	6.97	6.97E+02	0.84	1.2E+01	6.9
20	58.4	5.84	7.72E+02	0.67	1.5E+01	6.9
21	---	---	---	0.54	1.9E+01	6.8
22	41.2	4.12	1.02E+03	0.41	2.5E+01	7.3
23	---	---	---	0.34	3.0E+01	6.9
24	29.2	2.92	1.27E+03	0.26	3.8E+01	7.1
25	---	---	---	0.22	4.7E+01	6.7
26	20.5	2.05	1.59E+03	0.163	6.1E+01	7.1
27	---	---	---	0.131	7.7E+01	6.9
28	14.4	1.44	1.88E+03	0.105	9.5E+01	6.8
29	---	---	---	0.084	1.2E+02	6.7
30	10.2	1.02	2.35E+03	0.067	1.5E+02	6.7
31	---	---	---	0.054	1.9E+02	6.5
32	7.19	0.719	2.85E+03	0.043	2.3E+02	6.4
33	---	---	---	0.034	2.9E+02	6.4
34	5.12	0.512	3.64E+03	0.027	3.7E+02	6.4
35	---	---	---	0.022	4.7E+02	6.5
36	3.62	0.362	4.49E+03	0.018	5.8E+02	6.2
37	---	---	---	0.014	7.4E+02	6.2
38	2.5	0.25	5.27E+03	0.011	9.2E+02	6.1
39	---	---	---	0.009	1.2E+03	6.3
40	1.77	0.177	6.82E+03	0.007	1.5E+03	6.2

Table 3.2. Receiver coil parameters for different gauge enameled copper wires. Approximate size of the receiver coil diameter D = 1.343", length l = 0.5", thickness t = 0.0625".

Wire gauge	Turns per layer × No. of layers ($N_l \times N_t = N_R$)	Coil resistance R_R (Ω)	Coil inductance L_R (H)	Coil weight W_R (gm)	Parasitic capacitance C_{SR} (F)	Self-resonance frequency f_{SR} (Hz)
14	7 × 1 = 7	6.21E-03	2.11E-06	13.87	4.90E-13	1.57E+08
15	8 × 1 = 8	8.95E-03	2.75E-06	12.58	5.59E-13	1.28E+08
16	9 × 1 = 9	1.27E-02	3.48E-06	11.22	6.29E-13	1.08E+08
17	10 × 1 = 10	1.78E-02	4.30E-06	9.88	6.99E-13	9.19E+07
18	12 × 1 = 12	2.69E-02	6.19E-06	9.40	8.39E-13	6.99E+07
19	13 × 2 = 26	3.68E-02	7.26E-06	16.16	1.82E-12	2.19E+07
20	15 × 2 = 30	1.07E-01	3.87E-05	14.79	2.10E-12	1.76E+07
21	16 × 2 = 32	1.44E-01	4.40E-05	12.51	2.24E-12	1.60E+07
22	18 × 2 = 36	2.04E-01	5.57E-05	11.16	2.52E-12	1.34E+07
23	20 × 3 = 60	2.86E-01	6.88E-05	14.75	4.20E-12	6.25E+06
24	23 × 3 = 69	6.22E-01	2.05E-04	13.45	4.83E-12	5.07E+06
25	26 × 3 = 78	8.87E-01	2.61E-04	12.06	5.45E-12	4.22E+06
26	29 × 4 = 116	1.25E+00	3.25E-04	14.22	8.11E-12	2.32E+06
27	32 × 4 = 128	2.32E+00	7.04E-04	12.45	8.95E-12	2.01E+06
28	36 × 5 = 180	3.28E+00	8.91E-04	13.88	1.26E-11	1.20E+06
29	40 × 5 = 200	5.75E+00	1.72E-03	12.23	1.40E-11	1.03E+06
30	45 × 6 = 270	9.79E+00	3.13E-03	13.09	1.89E-11	6.55E+05
31	50 × 6 = 300	1.37E+01	3.87E-03	11.54	2.10E-11	5.59E+05
32	55 × 7 = 385	2.22E+01	6.37E-03	11.74	2.69E-11	3.85E+05
33	62 × 8 = 496	3.61E+01	1.06E-02	12.00	3.47E-11	2.63E+05
34	70 × 9 = 630	5.78E+01	1.71E-02	12.08	4.41E-11	1.84E+05
35	79 × 10 = 790	9.13E+01	2.68E-02	12.02	5.52E-11	1.31E+05
36	88 × 12 = 1056	1.41E+02	4.03E-02	12.74	7.38E-11	8.46E+04
37	98 × 13 = 1274	2.34E+02	6.98E-02	12.19	8.91E-11	6.39E+04
38	109 × 14 = 1526	3.54E+02	1.00E-01	11.58	1.07E-10	4.87E+04
39	125 × 17 = 2125	5.85E+02	1.72E-01	12.78	1.49E-10	2.97E+04
40	139 × 18 = 2502	9.22E+02	2.69E-01	11.94	1.75E-10	2.32E+04

Table 3.1 also includes the values of fusing current and the maximum allowed current in our design taken to be 10 % of the fusing current in the coil. Power dissipated (Pmax) when maximum allowed current passes through the coil is given by $I_{\max}{}^2 R_T$. Here, in this calculation the reflected impedance of the receiver coil on to the transmitter coil is neglected. When the power is restricted to 10 W, the maximum allowed current (Imax @ 10 W) passing through the coil is given by $\sqrt{10/R_T}$ and the maximum voltage (Vmax @ 10 W) that can be applied to the coil is given by $\sqrt{10R_T}$. For different wire gauge sizes the Pmax, Imax and Vmax are calculated and are shown in Table 3.1. The following considerations need to be given for selecting a particular coil design:

1. Transmitter coil input power and voltage criteria:

   Since the transmitter coil is to be worn by a patient around his/her waist, it should not get uncomfortably warm or need excessively high voltage. At this stage, the input power consumption in the transmitter coil for required output power at the receiver coil is not known. The maximum transmitter power at this stage is chosen arbitrarily as 10 W. The input voltage to the transmitter coil is also restricted to 110 V p-p (rms voltage = 38.9 V). Restricting the maximum input voltage (Vmax) applied to the coil to 38.9 V, from Table 3.1, any wire in the range of 10 – 24 gauge sizes can be chosen for transmitter coil.

2. Frequency of operation:

   The receiver coil induced voltage is high for a high operating frequency. As a rule of thumb the operating frequency is maintained at least 10 times less than the self-resonance frequency of the coil. Therefore the transmitter and the receiver coil with highest self-resonance frequency are chosen.

3. Receiver coil voltage criteria:

Producing voltage in excess of what is required in the receiver coil is a waste and may also be a concern from safety view point. The battery charging chip in this work requires a voltage in the range of 5 – 12 V dc. Hence the induced voltage in the receiver coil voltage is restricted to 15 V.

4. Receiver coil – power criteria:

   The receiver coil must supply 100 mA load current at 6.5 V to a battery charging chip. This implies an effective load of 65 Ω and load power of 650 mW. The power loss in the receiver coil must be kept as low as possible. The induced voltage needs to be regulated.

In this chapter, the design of the transmitter and the receiver coil is discussed. The various parameters for these coils using different gauge enamel coated copper wires are calculated. Finally various restrictions imposed on the coils are discussed.

4. ANALYSIS AND RESULTS OF COUPLED COILS FOR REMOTE POWER TRANSMISSION

The equivalent model for the wireless power transmission system is developed and analyzed in this chapter. The signal from an oscillator is used to drive the transmitter coil. The receiver coil picks up the transmitted power, and a circuit rectifies the induced voltage and converts it into a regulated dc supply for the implanted electronic system. A design procedure for the transmitter and receiving coil system is determined based on the load, frequency of operation and input supply voltage.

4.1 Analysis of Remote Power Transmission System

The wireless power transmission system is represented in Fig. 4.1. This system basically consists of a transmitter coil, a receiver coil, a rectifier circuit and the load. For the case under consideration, the latter is represented by the battery charging chip. The lumped equivalent models for the transmitter and the receiver coils are shown in Fig. 4.2 where lumped equivalent model of Fig. 2.1 is used for the inductor. Quantities L_T, R_T and C_{ST} are respectively the self inductance, the winding resistance and the parasitic capacitance of the transmitter coil. The operating frequency is chosen such that the transmitter and receiver coils are at resonance. Resonance is achieved by choosing suitable values for external capacitances C_T and $C_{RE.}$ Maximum coupling between the two coils of fixed geometry is achieved when both are tuned to resonate at the operating frequency. The resonance frequency is at least an order of magnitude lower than the self-resonance frequency of the transmitter coil. This allows for neglecting the parasitic capacitance C_{ST}. Hence the transmitter can be approximated as a series RLC circuit. Source voltage V_{IN} represents the rms input supply voltage. Similarly, L_R, R_R and C_{SR} respectively represent the self inductance, the winding resistance and the parasitic capacitance of the receiver coil. The receiver coil can be approximated as a parallel RLC circuit. An external

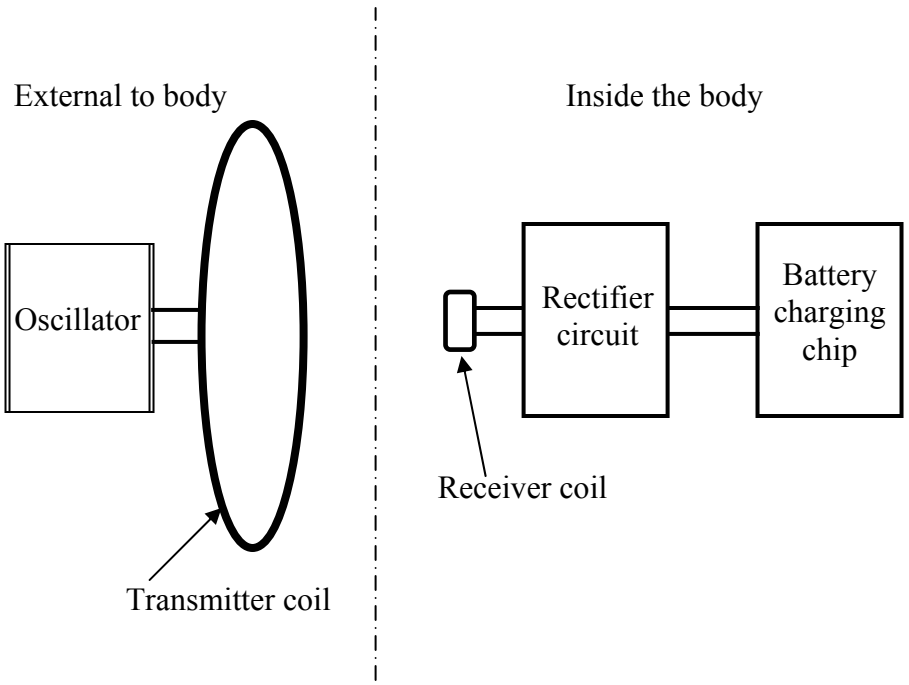

Fig. 4.1: System for inductively coupled remote power delivery.

capacitor C_{RE} is connected in parallel to the receiver circuit whose value is chosen such that receiver coil resonates at the operating frequency.

The induced voltage signal across the receiver coil is rectified by a full wave rectifier as shown in Fig. 4.2. This rectified signal is applied to the load as shown in Fig. 4.1. Here the load is a battery charging chip which requires a minimum dc current of 100 mA at a nominal dc voltage of 6.5 V. Hence the effective dc load resistance R_L is 65 Ω. The voltage across this R_L is smoothed by a large capacitor C_F whose value is chosen such that the ripple voltage across R_L is small. For the positive half cycle of the receiver coil voltage, diodes 1 and 3 conduct and the current charges the capacitor C_F and resistor R_L. During the next half cycle, diodes 2 and 4 send current through the capacitor C_F and resistor R_L. Since the filter capacitor will discharge during the time in-between peaks of the rectified waveform, it is important that the discharge time constant $R_L C_F$ be much greater than the period of the operating signal. This will ensure an almost constant voltage across the load resistor and the relation is given by

$$f_o >> \frac{1}{R_L C_F} \tag{4.1}$$

where, f_o is the operating resonance frequency in hertz. As long as Eq. 4.1 is true, the exact value of the filter capacitor does not affect the analysis. However, its value affects the load voltage.

A linear equivalent circuit for the rectifier, C_F and R_L is needed to analyze these coupled coils. When the voltage across the load is much greater than two forward conducting diode drops of 1.4 V, then it can be assumed that the rectifier acts as a peak rectifier with the peak value of voltage across $C_R = C_{SR} + C_{RE}$ appearing as a direct voltage across R_L. If the dc power dissipated in R_L, is equal to the ac power dissipated in the equivalent resistor placed directly in parallel with C_R and L_R, then the value of the equivalent resistor is $R_L/2$. The simplified version of Fig. 4.2 for the purpose of analysis is shown in Fig. 4.3.

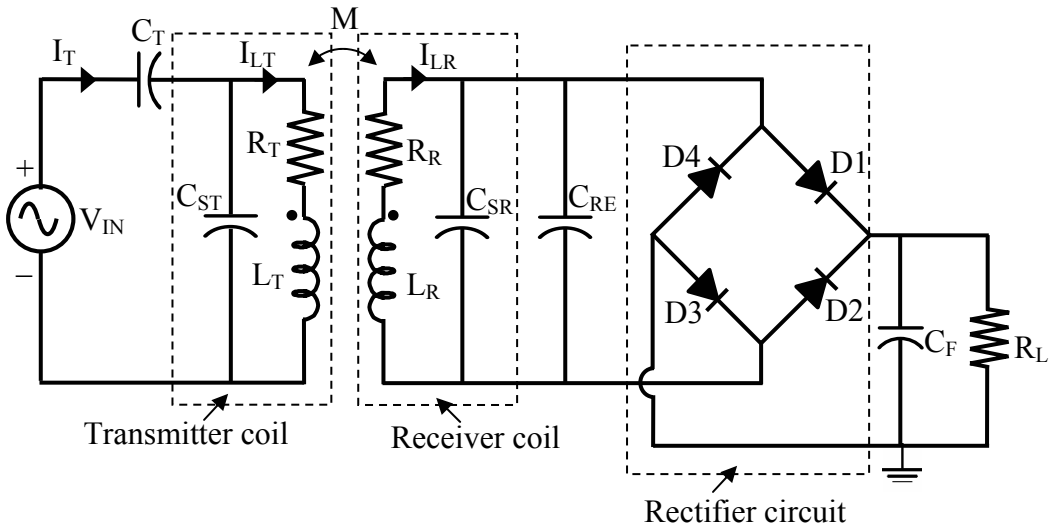

Fig. 4.2: Lumped equivalent model for wireless power transmission system.

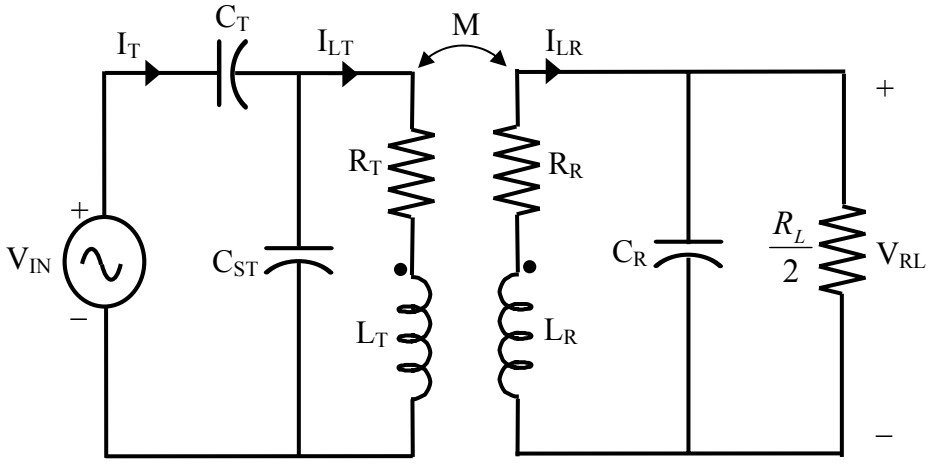

Fig. 4.3: Simplified version of model in Fig. 4.2 from power dissipation consideration. Here, $C_R = C_{SR} + C_{RE}$.

Here, the effect of the receiver coil on the transmitter coil and vice versa is neglected as they are loosely coupled. The impedance of the transmitter coil is approximated by:

$$Z_T = \frac{1}{j\omega C_T} + \frac{\left(R_T + j\omega L_T\right)\frac{1}{j\omega C_{ST}}}{R_T + j\omega L_T + \frac{1}{j\omega C_{ST}}} = R_{EQT} + jX_{EQT}$$

where,

$$R_{EQT} = \frac{R_T}{(1-\omega^2 L_T C_{ST})^2 + (\omega R_T C_{ST})^2} \text{ and}$$

$$X_{EQT} = \frac{\omega L_T (1-\omega^2 L_T C_{ST}) - \omega {R_T}^2 C_{ST}}{(1-\omega^2 L_T C_{ST})^2 + (\omega R_T C_{ST})^2} - \frac{1}{\omega C_T}. \quad (4.2)$$

At resonance $X_{EQT} = 0$ and $\omega = \omega_{OT}$. The value of the capacitor C_T is given by:

$$C_T = \frac{(1-{\omega_{OT}}^2 L_T C_{ST})^2 + (\omega_{OT} R_T C_{ST})^2}{{\omega_{OT}}^2 (L_T - {\omega_{OT}}^2 {L_T}^2 C_{ST} - {R_T}^2 C_{ST})}. \quad (4.3)$$

For a coil with $C_{ST} = 0$, $C_T = \frac{1}{{\omega_{OT}}^2 L_T}$ as expected for a series RLC circuit.

The impedance of the equivalent circuit on the receiver coil side is given by:

$$Z_R = \frac{1}{\frac{1}{R_R + j\omega L_R} + j\omega C_R + \frac{2}{R_L}} = R_{EQR} + jX_{EQR}$$

where,

$$R_{EQR} = \frac{R_R R_L \left(R_L + 2R_R\right) + 2\omega^2 {L_R}^2 R_L}{\left(R_L - \omega^2 L_R C_R R_L + 2R_R\right)^2 + \left(2\omega L_R + \omega C_R R_R R_L\right)^2} \text{ and}$$

$$X_{EQR} = \frac{\omega {R_L}^2 \left(L_R - C_R {R_R}^2 - \omega^2 {L_R}^2 C_R\right)}{\left(R_L - \omega^2 L_R C_R R_L + 2R_R\right)^2 + \left(2\omega L_R + \omega C_R R_R R_L\right)^2} \quad (4.4)$$

At resonance the $X_{EQR} = 0$ and $\omega = \omega_{OR}$, gives

$$C_R = \frac{L_R}{\omega_{OR}{}^2 L_R{}^2 + R_R{}^2} \text{ and the value of capacitor } C_{RE} = C_R - C_{SR}. \tag{4.5}$$

Now, for the coupled circuits, in Fig. 4.3, using KVL and KCL for the transmitter coil

$$V_{IN} = \frac{I_T}{j\omega C_T} + I_{LT}\left(R_T + j\omega L_T\right) - j\omega M I_{LR} \text{ and} \tag{4.6}$$

$$I_{LT} = I_T - \frac{I_{LT}\left(R_T + j\omega L_T\right) - j\omega M I_{LR}}{1/j\omega C_{ST}} \tag{4.7}$$

From Eqs. 4.6 and 4.7, we have

$$V_{IN} = I_{LT}\left(R_{ET} + jX_{ET}\right) - j\omega M I_{LR}\left(1 + \frac{C_{ST}}{C_T}\right)$$

$$\text{where } R_{ET} = R_T\left(1 + \frac{C_{ST}}{C_T}\right) \text{ and } X_{ET} = \omega L_T - \frac{1}{\omega C_T} + \omega L_T \frac{C_{ST}}{C_T}. \tag{4.8}$$

For the coupled circuits of Fig. 4.3,

$$\begin{bmatrix} V_{IN} \\ 0 \end{bmatrix} = \begin{bmatrix} R_{ET} + jX_{ET} & -j\omega M\left(1 + \frac{C_{ST}}{C_T}\right) \\ -j\omega M & R_R + j\omega L_R + \dfrac{\dfrac{1}{j\omega C_R}\dfrac{R_L}{2}}{\dfrac{1}{j\omega C_R} + \dfrac{R_L}{2}} \end{bmatrix} \begin{bmatrix} I_{LT} \\ I_{LR} \end{bmatrix} \tag{4.9}$$

$$\begin{bmatrix} V_{IN} \\ 0 \end{bmatrix} = \begin{bmatrix} R_{ET} + jX_{ET} & -j\omega M\left(1 + \frac{C_{ST}}{C_T}\right) \\ -j\omega M & R_{ER} + jX_{ER} \end{bmatrix} \begin{bmatrix} I_{LT} \\ I_{LR} \end{bmatrix}$$

$$\text{where } R_{ER} = R_R + \frac{2R_L}{4 + \omega^2 C_R{}^2 R_L{}^2}, \text{ and } X_{ER} = \omega L_R - \frac{\omega C_R R_L{}^2}{4 + \omega^2 C_R{}^2 R_L{}^2}. \tag{4.10}$$

From matrix inversion,

$$\begin{bmatrix} I_{LT} \\ I_{LR} \end{bmatrix} = \frac{1}{\Delta_R + j\Delta_X} \begin{bmatrix} R_{ER} + jX_{ER} & j\omega M \\ j\omega M\left(1 + \frac{C_{ST}}{C_T}\right) & R_{ET} + jX_{ET} \end{bmatrix} \begin{bmatrix} V_{IN} \\ 0 \end{bmatrix}$$

where, $\Delta_R = R_{ET}R_{ER} - X_{ET}X_{ER} + \omega^2 M^2\left(1 + \frac{C_{ST}}{C_T}\right)$ and $\Delta_X = X_{ET}R_{ER} + X_{ER}R_{ET}$. (4.11)

Thus, $I_{LR} = \frac{j\omega M V_{IN}\left(1 + \frac{C_{ST}}{C_T}\right)}{\Delta_R + j\Delta_X}$. (4.12)

The voltage V_{RL} and power P_{RL} across the load resistor are given by:

$$V_{RL} = I_{LR}\frac{\frac{1}{j\omega C_R}\frac{R_L}{2}}{\frac{1}{j\omega C_R} + \frac{R_L}{2}} = \frac{j\omega M V_{IN}\left(1 + \frac{C_{ST}}{C_T}\right)}{\Delta_R + j\Delta_X}\frac{R_L}{2 + j\omega C_R R_L}, \text{ and} \quad (4.13)$$

$$P_{RL} = \frac{V_{RL}^{\ 2}}{R_L/2} = \frac{2V_{RL}^{\ 2}}{R_L}. \quad (4.14)$$

4.2 Results of the Remote Power Transmission System

From the restrictions considered in section 3.3, transmitter coil with 10 gauge wire size was chosen since it has the highest self-resonance frequency compared to the other gauge wire sizes shown in Table 3.1. The parameters of the 57 turn transmitter coil are a winding resistance of 0.24 Ω, a self-inductance of 2.5 mH and an estimated parasitic capacitance of 47.6 pF. The maximum input supply voltage (rms) applied to the transmitter coil for a supply input power (P_{IN}) of 10 W is $V = \sqrt{P_{IN}R_T} \approx \sqrt{10 \times 0.24} = 1.55\ V_{rms}$. The self-resonance frequency of the transmitter coil is 462 kHz. From Table 3.2, if the self-resonance of the receiver coil is restricted to 462 kHz or higher, gauge sizes from 14 to 31 gauges are permissible for the receiver coil. Here, four different gauge sizes of 14, 20, 24 and 31 are selected for the receiver coil as a representative group to cover the entire possible range from 14 – 31 gauge sizes.

Equation 4.14, gives the dc power transferred to the 65 Ω load resistor, derived using the simplified model shown in Fig. 4.3. Figure 4.4 shows the dc power transferred to the load as a function of resonance frequency for the transmitter coil of 57 turns with respect to different receiver coil turns of 7, 30, 69 and 300 of wire gauge sizes of 14, 20, 24 and 31 respectively. For practical reasons, the operating frequency value chosen is at least 10 times less than the self-resonance of the transmitter coil, i.e., $f_o \leq 0.1 f_{OST}$. The self-resonance frequency of the transmitter coil is 462 kHz. The operating frequency for driving the transmitter coil in this work is selected to be 40 kHz, which is less than 46 kHz. From Fig. 4.4, it can be observed that the maximum power transfer to the 65 Ω load resistor occurs for the receiver coil with N_R = 30 at frequencies greater than about 20 kHz for transmitter coil with N_T = 57. The winding resistance, self-inductance and parasitic capacitance of the 30 turn receiver coil are respectively 0.146 Ω, 38.7 μH, and 2 pF. The self-resonance frequency of the 30 turn receiver coil is 17.6 MHz.

Figure 4.5 shows the variation of the DC power as a function of rms value of the input supply voltage V_{IN}. The required receiver power of 650 mW for a 57 turn transmitter coil and a 30 turn receiver coil can be theoretically obtained for input rms supply voltage of 0.85 V provided there are no other losses in the system. For operating frequency of the 40 kHz, the values of external capacitors C_T and C_{RE} connected to the transmitter and the receiver coil as shown in Fig. 4.3 are respectively 6.3 nF and 0.4 μF. For the input supply voltage of 0.85 V the estimated rms voltage across the $R_L/2$ resistor is 4.6 V which is equal to peak voltage of 6.5 V. The rms current passing through the $R_L/2$ resistor is 141.5 mA. A practical system will have losses and hence a higher input voltage to the transmitter coil will be necessary.

Figure 4.6 shows the fabricated coils. From section 3.1, the number of turns along the length and thickness of the transmitter coil are 19 and 3 respectively. However, during

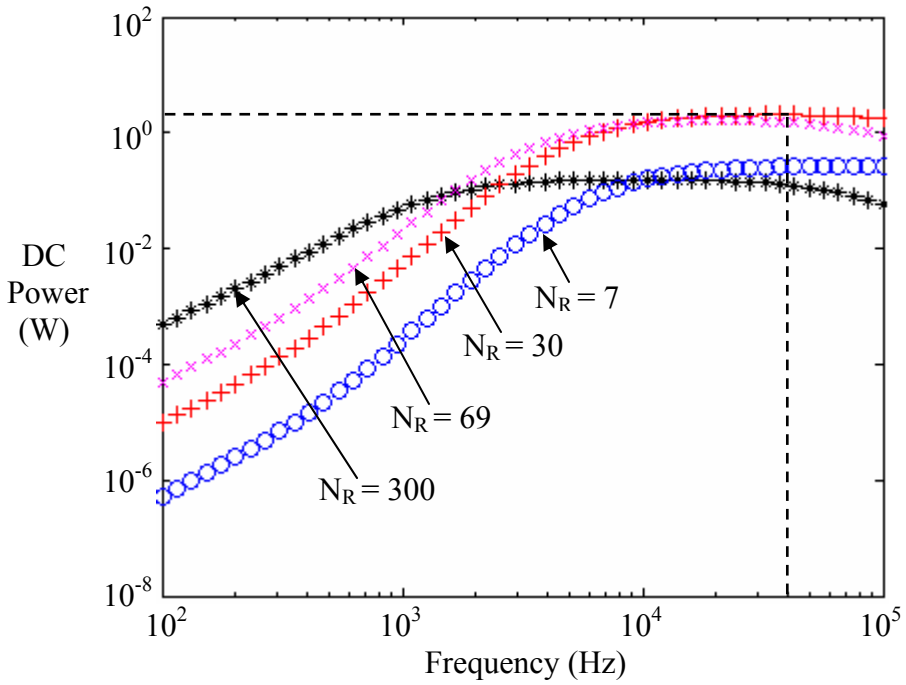

Fig. 4.4: DC power transferred to the 65 Ω load resistor as a function of resonance frequency. Transmitter coil turns N_T = 57, transmitter coil wire gauge number = 10. Receiver coil turns of N_R = 7, 30, 69 and 300 for receiver coil wire gauge number of 14, 20, 24 and 31 respectively. The rms value of supply voltage to the transmitter (V_{IN}) is 1.5 V.

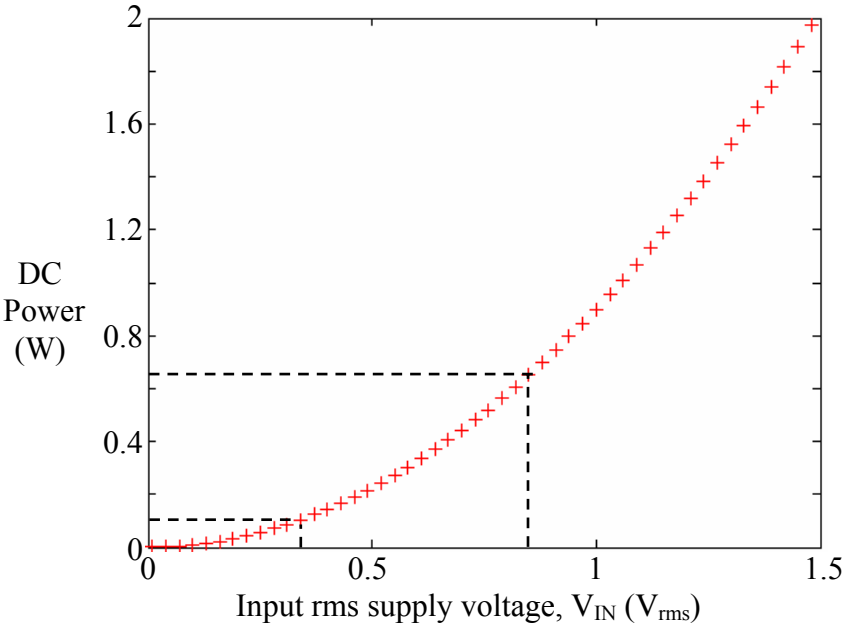

Fig. 4.5: DC power transferred to the 65 Ω load resistor as a function of input rms supply voltage. Transmitter coil turns N_T = 57, transmitter coil wire gauge number = 10. Receiver coil turns of N_R = 30, receiver coil wire gauge number = 20. The operating resonance frequency is 40 kHz. For V_{IN} of 0.35 V, DC power transferred to the 65 Ω load resistor is 0.11 W.

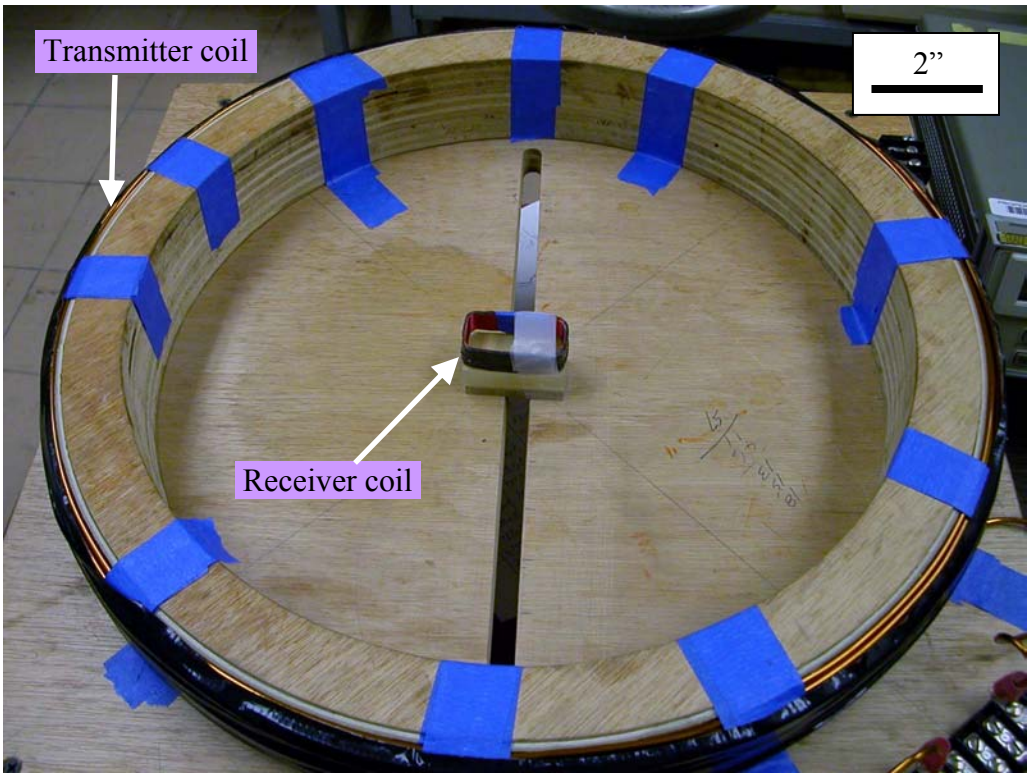

Fig. 4.6: Fabricated transmitter and receiver coils.

fabrication of the coil due to imperfect winding process, it required four layers to obtain 57 turns. For the receiver coil, the number of turns along the length and thickness are 15 and 2 respectively. During fabrication the 30 turn receiver coil required three layers. The measured values of the self-inductances and the winding resistances of the transmitter and receiver coils as a function of frequency are shown in Figs. 4.7 and 4.8 respectively. The value of inductance of transmitter coil is almost constant in frequency range of 100 Hz to 40 kHz. Its value at 100 Hz and 40 kHz are respectively 2.4 mH and 2.47 mH. The measured resistance values of transmitter coil are almost constant for the frequencies below 1 kHz and the values are slightly higher than the theoretical value. The measured resistance value of the transmitter coil increased with increase in the frequency. The values of the winding resistance of the transmitter coil are respectively 0.356, 0.353, 0.363, 0.38, 0.485, 0.746, 1.496, 3.56, 5.99 and 11.5 Ω at frequencies of 100, 120, 200, 400, 1 k, 2 k, 4 k, 10 k, 20 k and 40 kHz. The value of the inductance of the receiver coil is almost constant in the frequency range of 100 Hz to 40 kHz. Its values at 100 Hz and 40 kHz are respectively 39.4 μH and 38.85 μH. The value of the winding resistance of the receiver coil is almost constant of 0.169 Ω in the frequency range of 100 Hz to 2 kHz. Its value at 4 k, 10 k, 20 k and 40 k Hz are respectively 0.172, 0.188, 0.241, 0.405 Ω.

The increase in the effective resistance of the transmitter coil in Fig. 4.7 (b) can be attributed to skin effect. Skin depth (δ) of the conductor is defined as the depth at which conductor's current is reduced to 1/e i.e., 37 % of surface value and is given by

$$\delta = \sqrt{\frac{1}{\pi f \sigma \mu}} \tag{4.14}$$

where, σ is the wire conductivity, f is the signal frequency in hertz and μ is the magnetic permeability of copper. The conductivity and the permeability of the copper wire are respectively

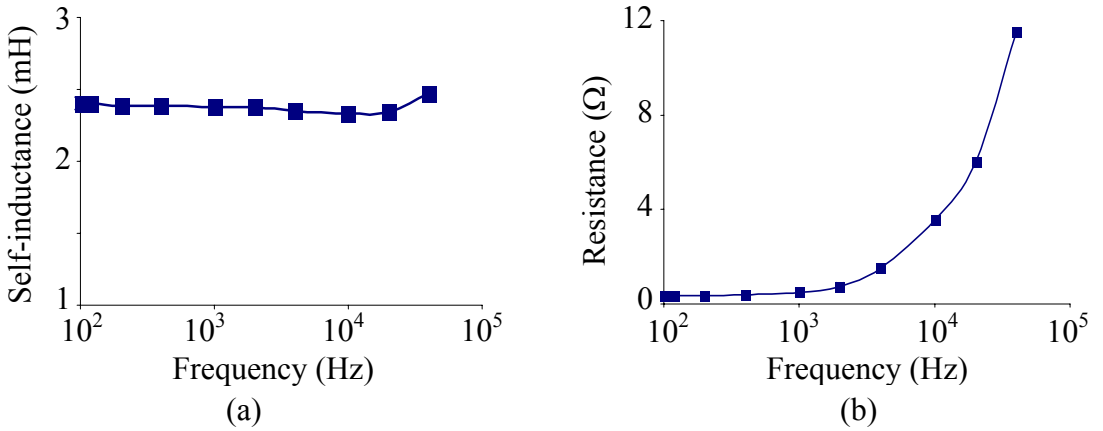

Fig. 4.7: (a) Self-inductance and (b) Winding resistance of the transmitter coil at frequencies below self-resonance frequency.

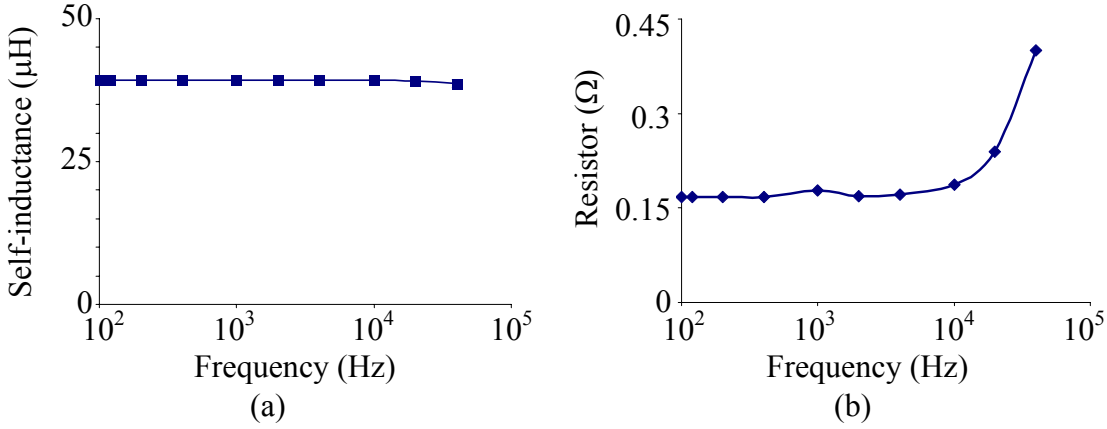

Fig. 4.8: (a) Self-inductance and (b) Winding resistance of the receiver coil at frequencies below self-resonance frequency.

574530 Ω^{-1} cm^{-1} and $4\pi\times10^{-9}$ H cm^{-1}. At low frequencies, current flows through the entire cross section of a copper conductor. As the frequency increases, current concentrates near the surface of the conductor. Table 4.1 gives the skin depth values of copper conductor at different frequencies. The value of skin depth decreases with the increase in frequency. From Table 4.1, at 2.6 kHz frequency, the value of the skin depth is 0.13 cm, which is equal to the radius of 10 gauge copper wire. At a frequency higher than 2.6 kHz, the effective cross-section for current flow in the transmitter coil will decrease and hence the wire effective resistance increases as is evident from Fig. 4.7 (b). At a frequency of 26 kHz, the value of the skin depth value is 0.0412, which is equal to the radius of 20 gauge copper wire. Beyond 26 kHz, the receiver coil effective resistance increases as seen from Fig. 4.8 (b).

At the frequency of 40 kHz, the measured resistance of the transmitter and receiver coils is respectively 11.5 Ω and 0.4 Ω. The estimated low frequency dc resistance values of the transmitter and receiver coils are respectively 0.24 Ω and 0.146 Ω. At low frequencies the measured values of the transmitter and receiver coils are respectively 0.356 Ω and 0.168 Ω which are comparable with dc values. The actual value of the load resistor, external capacitors C_T and C_{RE} used for measurements are respectively 68 Ω, 6.7 nF and 0.45 μF. Neglecting the rectifier circuit as shown by the simplified model in Fig. 4.3, the experimental values were measured.

Figure 4.9 shows the experimental setup for the remote transfer of the power. The transmitter and the receiver coils were observed to resonate at frequencies of 39.45 kHz and 39.7 kHz, respectively. This mismatch in the resonating frequency of the receiver and transmitter coils is due to the difference in the computed and standard values of external capacitors C_T and C_{RE}. Figure 4.10 shows the transmitted power to the load of receiver coil as a function of the

Table 4.1: Skin depth values of copper at different frequencies.
10 gauge copper wire (radius = 51.2 mil = 0.13 cm).
20 gauge copper wire (radius = 16.3 mil = 0.0414 cm).

Frequency (kHz)	Skin depth δ (cm)
0.1	0.6643
0.5	0.297
1	0.21
2.6	0.13
5	0.094
10	0.0664
20	0.047
26	0.0412
40	0.0332
50	0.0297

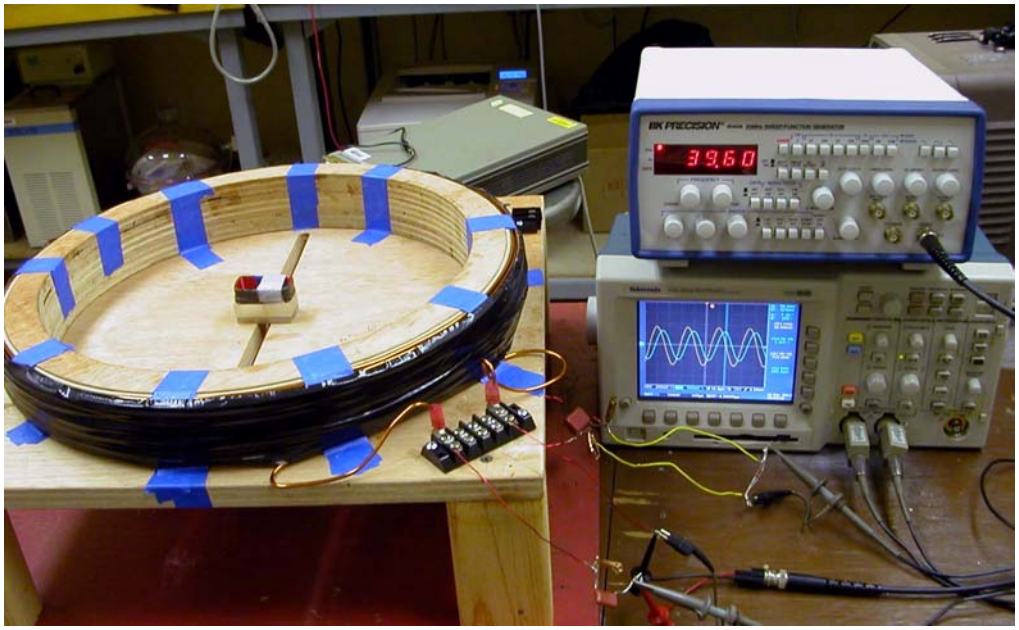

Fig. 4.9: Experimental setup for the remote power transfer.

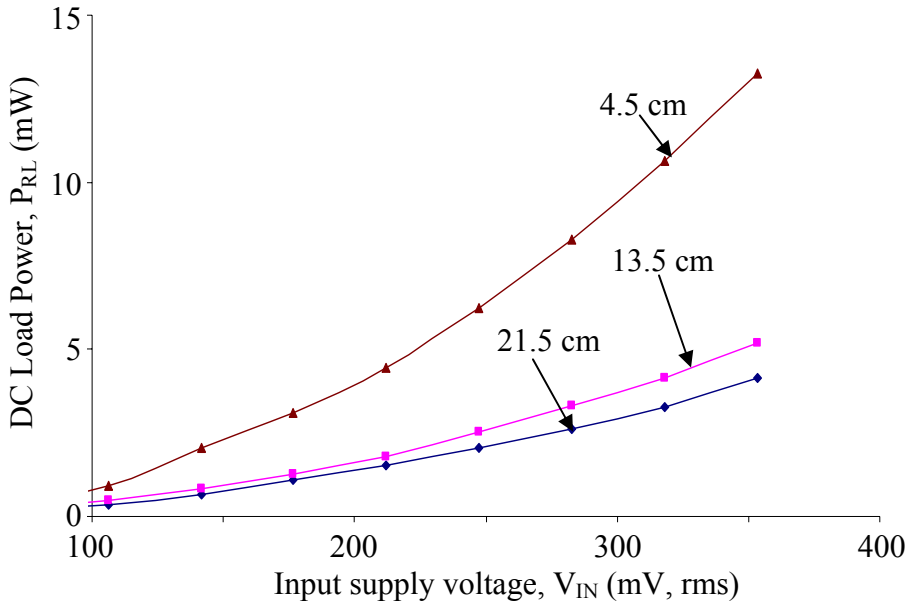

Fig. 4.10: Measured power transmitted to the load resistor as a function of input supply voltage for a 57 turn transmitter coil and 30 turn receiver coil at an operating frequency of 39.45 kHz. The numbers shown in the plot along with the curve indicate the distance between the center of the receiver coil and the rim of the transmitter coil of diameter 43 cm.

both the input supply voltage V_{IN} and the position of receiver coil along the axis of the transmitter coil.

The maximum value of rms supply voltage obtained from the oscillator to drive the transmitter coil was 0.35 V at the operating frequency of 39.45 kHz. For an input rms supply voltage of 0.35 V, the observed voltage across the 34 Ω ($R_L/2$) resistor was 0.37 V, when the receiver coil was placed at the center of the transmitter coil. When the receiver coil is moved laterally to the rim of the transmitter coil, the observed rms voltage across the 34 Ω resistor was 0.67 V for the same input rms supply voltage of 0.35 V. This is because the coupling between a transmitter and a receiver coil placed coaxially at the center is just over one-half the value achieved when the receiver coil is placed near the perimeter of the transmitter coil [7]. Hence the transmitted power to the load of the receiver coil is 4 mW when the receiver coil is placed at the center and its value is 13.2 mW when the latter is placed at the rim of the transmitter coil. These measured values are significantly lower than the theoretically calculated value of 0.11 W in Fig. 4.5.

For an input rms supply voltage of 0.35 V, the expected theoretical value of the induced voltage across the load resistor of the receiver coil using the actual values is 69 mV (rms) and the power transferred to the load resistor is 0.14 mW. The value of the mutual inductance given by Eq. 2.26, assumes that the coils are perfectly aligned. It gives a slightly lower coupling value than expected in practice [16]. The increase is the induced voltage might be due to the increase in the value of mutual inductance when the coils are brought in proximity of each other.

The power transferred to the receiver coil can be increased by increasing the input supply voltage to the transmitter coil. The rectifier circuit can not be used at this stage since the voltage obtained across the load resistor is small so that we can not neglect the two forward conducting diode drops discussed in the section 4.1.

In this chapter, the remote power transmission system is analyzed. All the assumptions made to arrive at the simplified model are discussed in detail. The results obtained for the remote power transmission system are presented.

5. DESIGNING OF OPERATIONAL AMPLIFIER

A CMOS operational amplifier (op-amp) is designed for amplifying differential signal from a MEMS sensor such as a laterally movable gate field effect transistor (LMGFET) accelerometer [17]. The op-amp is fabricated first on the chip prior to the accelerometer fabrication. The latter utilizes a post-IC processing technique to achieve monolithic integration of a sensor with circuitry. Op-amp is suitable for amplifying a differential analog signal output from the accelerometer. Choice of an op-amp for amplification provides typical advantages of high-differential gain, high rejection of common-mode signal due to temperature and other drifts common to both devices, high input impedance and low output resistance.

5.1 Op-Amp Design Methodology

The op-amp is designed to amplify the sensor output signal. The differential output voltage of the LMGFET accelerometer to be sensed is expected to be in mV range with a bandwidth of at least 20 kHz. A two-stage CMOS amplifier is considered for the op-amp design. The four functional blocks used in the design are shown in Fig. 5.1. First block is an input differential gain amplifier. The second block converts the differential signal into a single-ended signal, since subsequent block have inputs that are referenced to ground. DC level-shift is used for proper biasing of the second gain stage, which provides additional gain. Circuit implementation of op amp is shown in Fig. 5.2 [18]. The description as well as the design methodology for each of the block mentioned above is explained in the following subsections.

5.2 Design of Differential Amplifier

The first block in the op-amp design is a differential amplifier which plays an essential role in analog integrated circuits (IC) design, as it is capable of amplifying the difference between two inputs and rejecting the signals that are common to both inputs. Examples of the

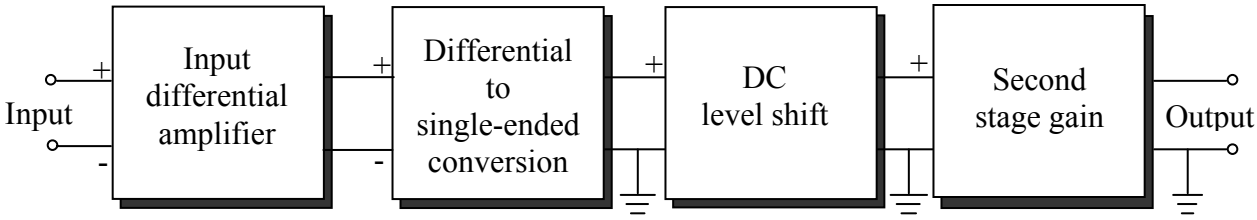

Fig. 5.1: Block diagram for an integrated op-amp.

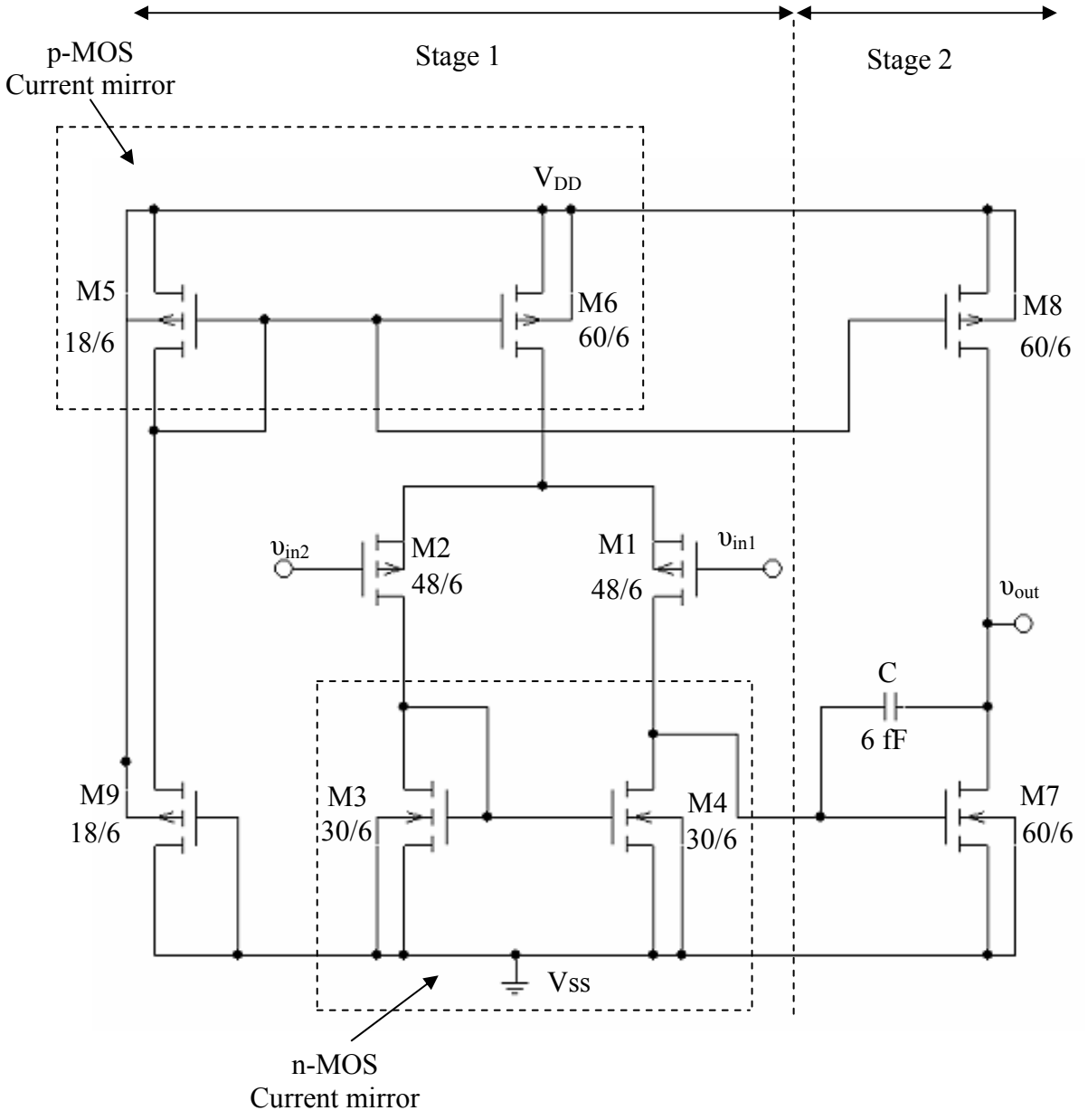

Fig. 5.2: The two-stage CMOS op-amp circuit diagram.

unwanted common-mode signals include common noise signal, variation in the power supply voltage as a function of time, variation in the substrate voltage with time and the variation in the temperature of the IC. The current mirror, an important component of the op-amp is discussed briefly followed by the discussion of the differential amplifier.

- **Current Mirror:**

Current mirror is an extension of a current source/sink circuit and is used extensively in MOS analog ICs as a biasing element. The current mirror makes use of the fact that if the gate-to-source potentials of two identical MOS transistors are equal, then their channel currents should be equal [19]. Figure 5.3 (a) & (b) show the implementation of n-MOS and p-MOS current mirrors. The p-MOS mirror serves as a current source while the n-MOS mirror acts as a current sink. When the gate is tied to its drain, an enhancement mode transistor operates in saturation. The voltage developed across the diode-connected transistor M3 is applied to the gate and source of the second transistor M4, which provides a constant bias current I_O. The current I_I is defined by a current source and I_O is the output or "mirrored" current. The current ratio I_O/I_I is determined by the aspect ratio (W/L) of the transistors where W is the channel width and L is the channel length.

In Fig. 5.3 (a),

$$\frac{I_O}{I_I} = \frac{L_3}{W_3} \times \frac{W_4}{L_4}. \tag{5.1}$$

During fabrication, channel length can be varied substantially. However, the most accurate current ratio is usually obtained when the devices of the same channel length L are used. For this case, the ratio of currents is then set by the channel width W. As a result, Eq. 5.1 for same channel length simplifies to

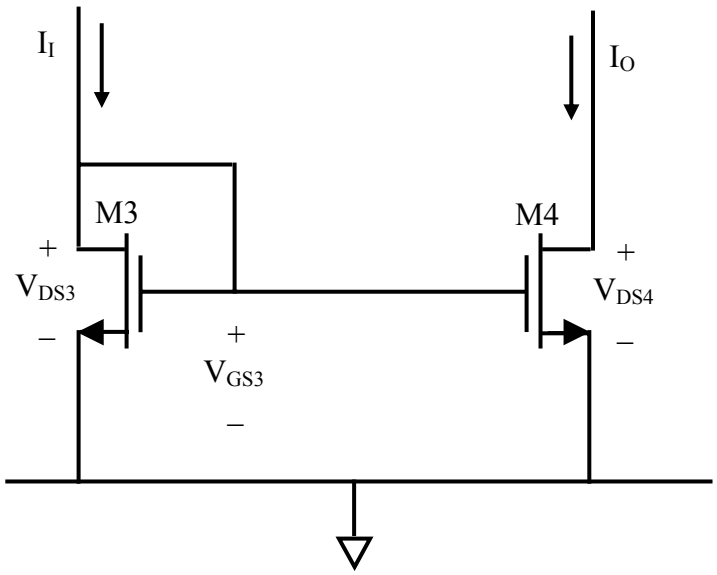

(a)

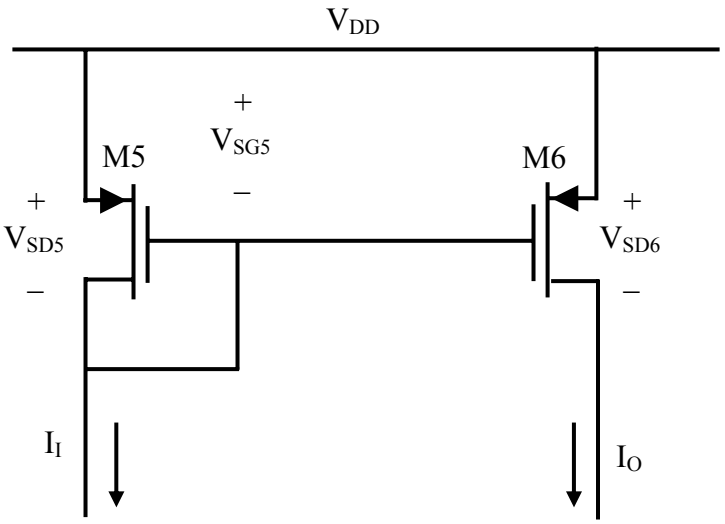

(b)

Fig. 5.3: (a) n-MOS and (b) p-MOS current mirrors.

$$\frac{I_O}{I_I} = \frac{W_4}{W_3}. \tag{5.2}$$

Similarly for Fig 5.3 (b) for equal channel lengths

$$\frac{I_O}{I_I} = \frac{W_6}{W_5}. \tag{5.3}$$

The design of the first two functional blocks of the op-amp in Fig. 5.1 is discussed here. Figure 5.4 shows the design implementation of the single-ended output differential amplifier. The p-MOS transistors M1 & M2 form the differential input pair for the differential amplifier with their sources tied together. Empirical observations show that p-channel devices have lower noise than n-channel devices of equivalent size and bias conditions [20]. Since the first stage of any cascaded amplifier should have the lowest possible noise so that it is not amplified by subsequent stages, p-channel transistors are chosen for M1 and M2. The n-MOS transistors M3 & M4 act as an active load for the differential amplifier and also provide conversion of the differential signal to a single-ended output signal. Excluding biasing transistors, four transistors M1, M2, M3 and M4 implement the first two functional blocks in Fig. 5.1. The combination of transistors M5 and M6, with the connections shown, forms a current mirror. The biasing for the differential amplifier is set by this current source. Reference current mirrored in transistor M6 depends on the width ratio of transistors M6 and M5 for equal channel lengths. The p-MOS transistor M9 sets the reference current. The transistor M9 acts as an active resistor as its gate and drain are connected as shown in Fig. 5.4 and is always in saturation mode of operation. The substrate of p-channel transistors is connected to positive terminal V_{DD} and the substrate of n-channel transistors is connected to most negative terminal V_{SS}.

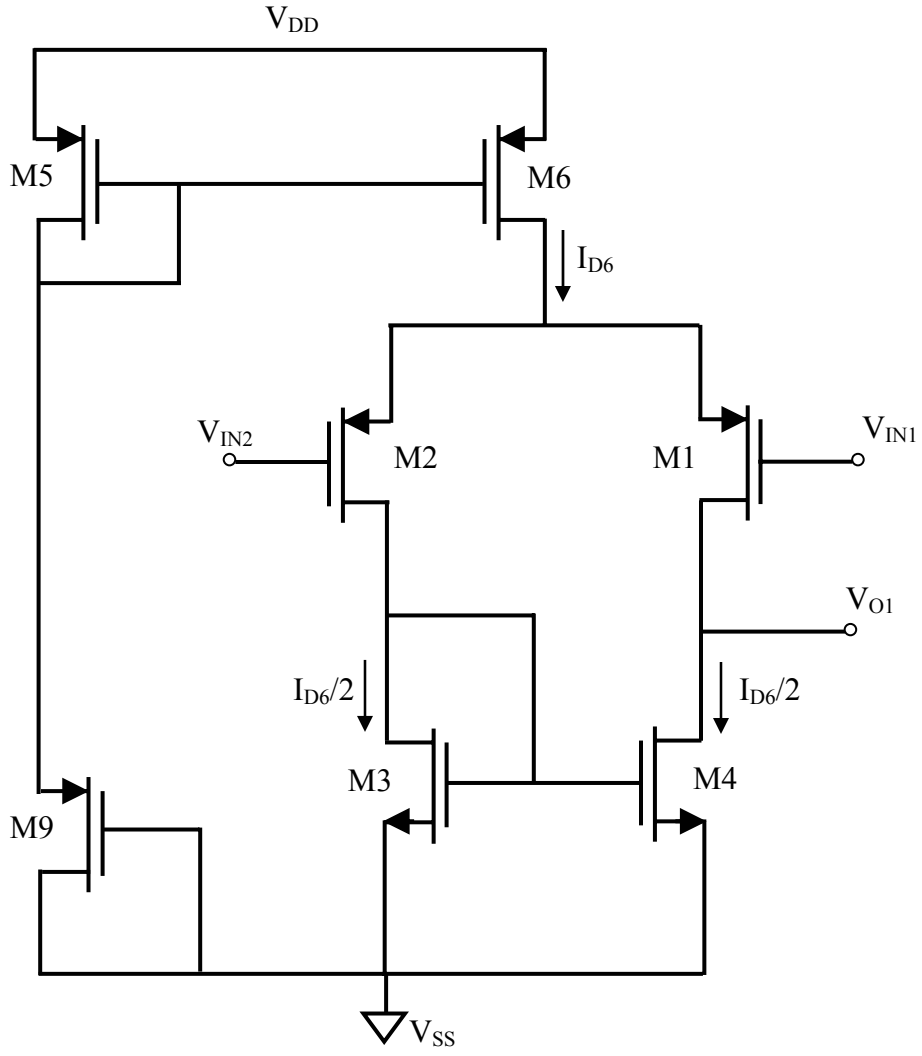

Fig. 5.4: Differential input, single-ended output differential amplifier.

5.3 Dc Level Shift and Second Stage Gain

Next, the dc level-shifting function is considered. Assuming that in the Fig. 5.4 the transistor pairs (M1, M2) and (M3, M4) are individually perfectly matched, the drain currents are $I_{D6}/2$ for M1 & M2 and $I_{D6}/2$ for M3 & M4. $V_{GS3} = V_{DS3}$ as the transistor M3 is diode-connected and its drain current I_{D3} is given by [18]

$$I_{D3} = \frac{1}{2}\mu_n C_{ox}\left(\frac{W}{L}\right)_3 \left(V_{GS3} - V_{Tn}\right)^2 \left(1 + \lambda_n V_{DS3}\right) = \frac{I_{D6}}{2}. \tag{5.4}$$

Here $(W/L)_x$ denotes the aspect ratio W/L for transistor X, μ_n and μ_p are channel mobility of the electrons and holes respectively, C_{ox} is the oxide capacitance per unit area, V_{Tn} and V_{Tp} are the threshold voltages of n-channel and p-channel MOSFETs respectively, and λ_n and λ_p are the channel-length parameters for n-channel and p-channel transistors respectively. Since $V_{DS3} = V_{GS3}$, and designing $(W/L)_4 = (W/L)_3$, the drain current I_{D4} through M4 is,

$$I_{D4} = \frac{1}{2}\mu_n C_{ox}\left(\frac{W}{L}\right)_4 \left(V_{GS4} - V_{Tn}\right)^2 \left(1 + \lambda_n V_{DS4}\right) = \frac{I_{D6}}{2}. \tag{5.5}$$

Equating Eqs. 5.4 & 5.5, we get $V_{DS4} = V_{GS3}$. For perfect matching, the current-mirror transistors must have the same drain-to-source voltages and identical gate-to-source voltages. Neglecting channel length modulation λ_n, we get from Eq. 5.4

$$V_{DS4} = V_{GS3} = V_{Tn} + \sqrt{\frac{I_{D6}}{\mu_n C_{ox}\left(W/L\right)_3}}. \tag{5.6}$$

The first-stage output dc bias voltage V_{O1} in Fig. 5.4 with both the inputs $V_{IN1} = V_{IN2} = 0$ with respect to ground is given by

$$V_{O1} = V_{SS} + V_{DS4} \approx V_{SS} + V_{Tn} + \sqrt{\frac{I_{D6}}{\mu_n C_{ox}\left(W/L\right)_3}}. \tag{5.7}$$

For identical (M1, M2) and (M3, M4) pairs, the small signal single-ended differential gain of the first-stage can be given by

$$A_{v1} = \frac{g_{m1}}{g_{m1} + g_{m4}} \tag{5.8}$$

where $g_{m1}$and g_{m4} are the transconductance parameters of transistors M1 and M4 respectively. Since the first-stage output is one gate-source potential above the negative supply, the next stage must shift the dc level towards the positive supply voltage. The level-shift function can either be accomplished with a p-channel source follower or by an n-channel MOSFET connected as a common-source amplifier. But the choice of n-channel MOSFET accomplishes added gain in a single stage along with level-shifting. Transistors M7 and M8 in Fig. 5.2 implement the last two functional blocks in the Fig. 5.1. The single-ended differential output from the differential pair (M1 & M2) is the input signal to the common source amplifier M7. Current mirror comprising of transistors M5, M8 and M9 biases the second gain stage. A p-channel current supply (M8) is used to maximize the second-stage gain which acts as active load for M7. The gain of second-stage can be expressed as

$$A_{v2} = \frac{-g_{m7}}{g_{m7} + g_{m8}}. \tag{5.10}$$

The open-circuit differential gain, obtained from the cascade of first and second stages is $A_{\upsilon} = A_{\upsilon 1} \times A_{\upsilon 2}$.

A feedback capacitor C is added between the drain and gate of the output transistor M7. The role of this capacitor is to ensure stable operation with adequate phase margin. Since some amount of feedback is always present in any amplifier due to parasitics, the total loop phase shift may become 0° or 360°, making the feedback positive. If the gain at this frequency is greater than unity, oscillations result rather than amplification. Thus an important part of the amplifier

design is to ensure that the gain of the amplifier is less than unity, at the frequency where the phase shift is zero. With the compensation capacitor C, the op-amp provides gain with good frequency response. The simulated values of the frequency and phase response of op-amp for different values of compensation capacitor C are shown in Fig. 5.5. The unity gain bandwidth and the phase shift vary with the value of C. Here, the lowest value capacitance is used as compensation capacitor because it occupies less space on the chip.

In order to specify the bias current and the transistor dimensions, constraints has to be placed on the dc supplies and the total dc power dissipation for the op-amp. In this design, the dc supplies are V_{DD} = 5 V and V_{SS} = 0 V since the fabrication process restricts the operating voltage to 5 V. The dc power dissipation is arbitrarily chosen as 2.3 mW. As a result, the dc supply currents must add to no more than 2.3 mW/5 V = 460 μA. In 1.5 μm technology utilized for fabrication, the minimum channel length of a transistor is 1.5 μm. The length of the transistor in the design must be greater than the minimum channel length to avoid short channel length effects of the transistor [21]. Minimum channel length of 6 μm is selected in this work. The input transistor pair is biased at $I_{D6}/2$ = 100 μA in order to have adequate first stage gain. Transistor M7 is biased at I_{D7} = 200 μA and has $(W/L)_7$ = 10. The current source M9 is then limited to consume the remaining 60 μA. In order to avoid systematic input offset voltage, the current densities in the transistor are kept the same. This determines the limitation of transistors M3 and M4 as

$$\frac{(W/L)_7}{2(W/L)_{3,4}} = \frac{I_{D7}}{I_{D6}} = 1 \qquad \text{or} \qquad \left(\frac{W}{L}\right)_{3,4} = \frac{1}{2}\left(\frac{W}{L}\right)_7 = 5\,. \tag{5.11}$$

5.4 Simulation Results

The designed operational amplifier as shown in the Fig. 5.2 is simulated using PSPICE.

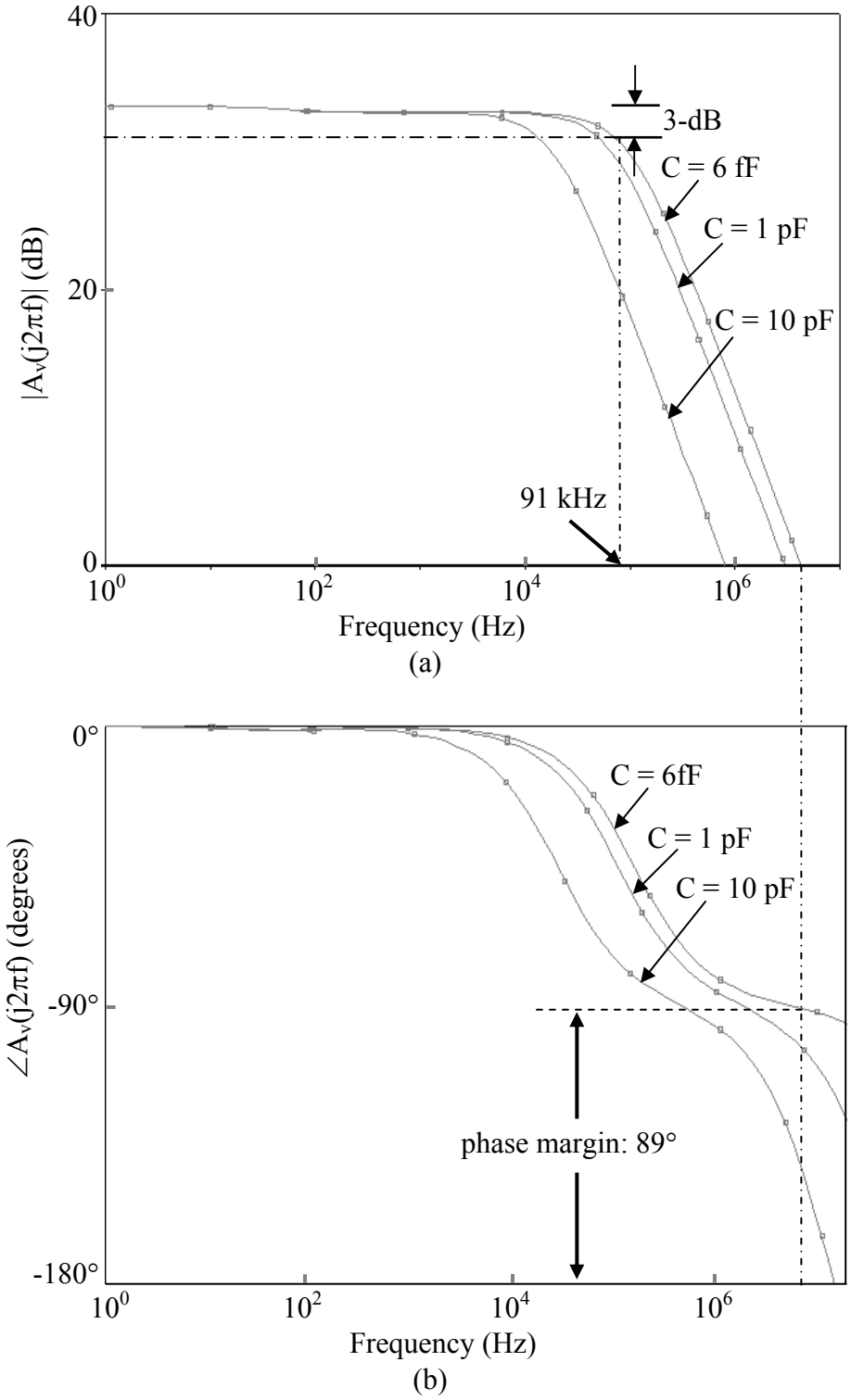

Fig. 5.5: Effect of compensation capacitor C of op-amp on (a) frequency response and (b) phase response.

Level-3 MOS model parameters were used in the simulations. The physical layout of the op-amp is done using Tanner L-EDIT 8.20 and various interlayer capacitances were extracted from the layout. These capacitances were included in the simulation program for more reliable results. The layout of the op-amp is shown in Fig. 5.6. The numbers in Fig. 5.6 describe the channel width to length (W/L) ratios of the MOS transistors in μm. The PSPICE 'net list' file used for simulating the op-amp is included in Appendix B. Figure 5.7 shows the microscope picture of the fabricated op-amp. Figure 5.8 shows the steady state ac simulation response of the input signal amplitude. For a 48 mV peak-to-peak differential input shown in Fig. 5.8 (a), the peak-to-peak output of the op-amp obtained is 2.18 V as shown in the Fig. 5.8 (b), giving a gain of 45.4 (33.14 dB). From Fig. 5.5 (a) the 3-dB bandwidth of 91 kHz is obtained for the op-amp from simulations. Requirement for the op-amp to be stable is that the gain curve cross the 0 dB point before the argument of the gain reaches 180°. A measure of stability is given by the value of the phase when gain is unity i.e., 0 dB and this measure is called phase margin. From simulation results shown in Fig. 5.5 (b) a phase margin of 89° is attained with 6 fF compensation capacitor. Larger phase margins result in less "ringing" of the output signal which is desirable. It is desirable to have a phase margin of at least 45° to keep the ringing to an acceptable level.

Experimental measurements were made on the fabricated op-amp with 18 mV peak-to-peak signal applied to the differential input. Observed gain was only 3 (9.5 dB) and the measured 3-dB bandwidth was 1 MHz. The experimental results did not match with the design simulations. This is attributed to differences in the MOS model parameter values used in the simulations compared to the values appropriate for the process utilized by the foundry. Table 5.1 compares the MOS model parameter values used in the simulation to that used during fabrication. When simulations were redone using the parameter values given by the foundry, the new value for gain

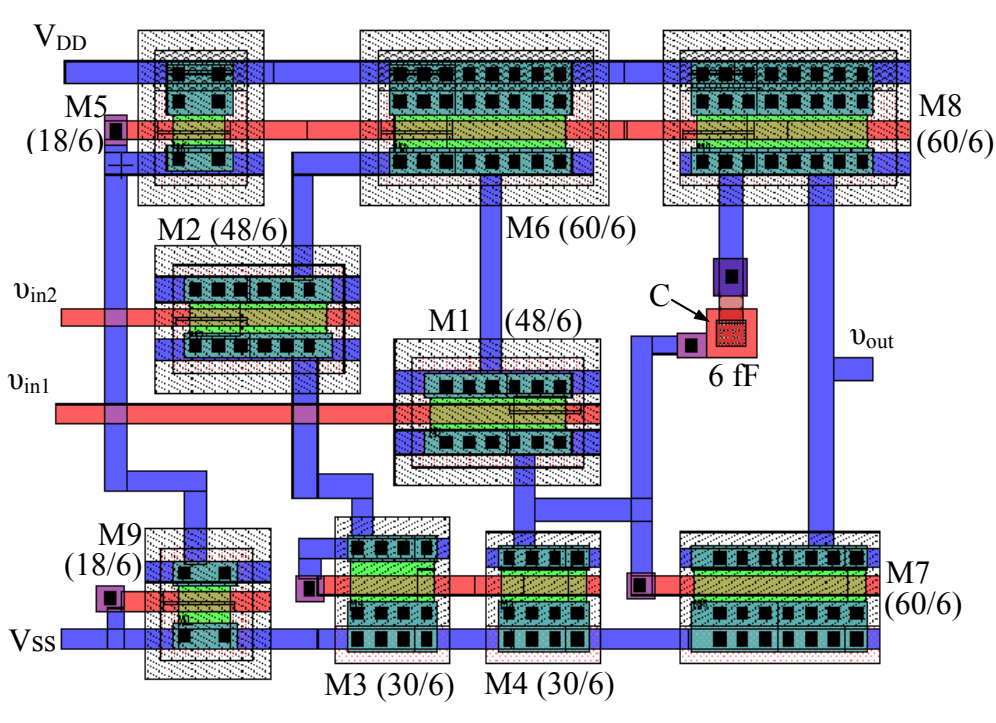

Fig. 5.6: Layout of the op-amp design in Fig. 5.2 in L-EDIT 8.20.

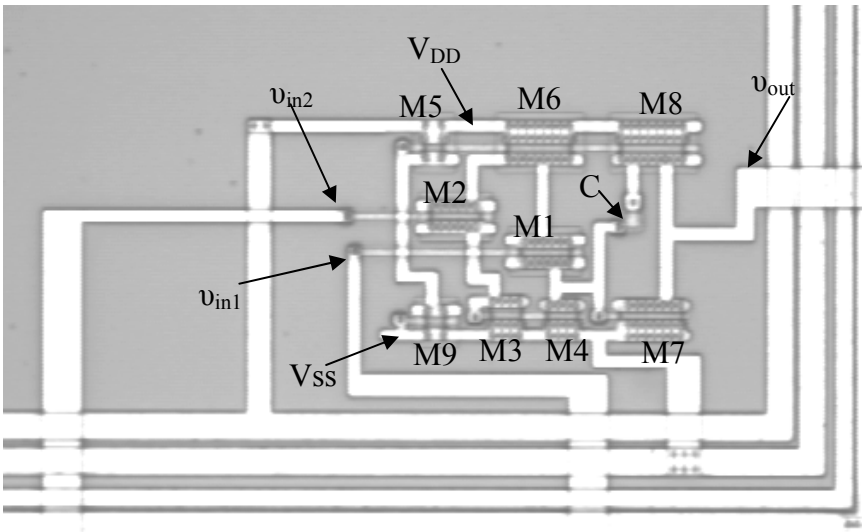

Fig. 5.7: Microscope picture of the fabricated op-amp utilizing a 1.5 µm standard CMOS process.

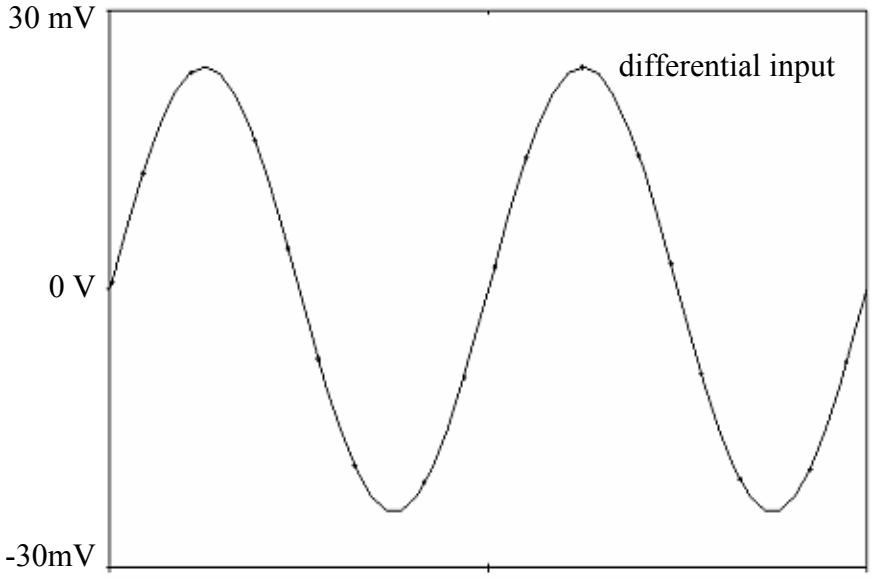

(a)

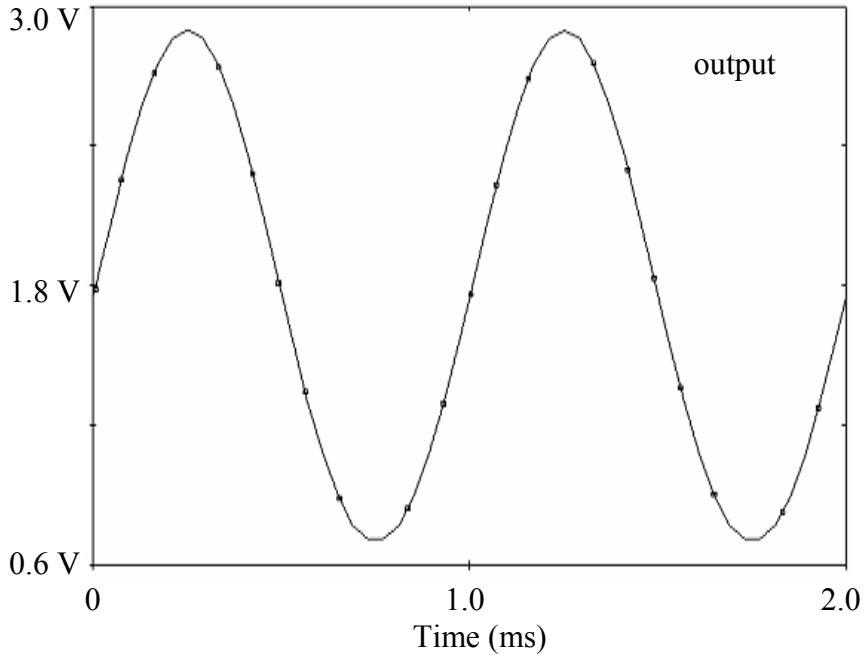

(b)

Fig. 5.8: Steady state ac response for high input signal amplitude.
(a) differential input signal and (b) output signal of the op-amp.

Table 5.1: Level-3 MOS model parameters of the simulated and fabricated chip.

Parameters	Fabricated		Simulated	
	NMOS	PMOS	NMOS	PMOS
Thin oxide thickness	3.2E-08	3.2E-08	3.1E-08	3.1E-08
Substrate doping	4.0E+15	1.0E+17	2.3E+16	6.4E+15
Body-effect parameter	0.709	0.51	0.782	0.409
Surface inversion potential	0.7	0.7	0.7	0.7
Zero-bias threshold voltage	0.597	-0.889	0.687	-0.757
Width effect on threshold voltage	0.428	0.407	0.0	2.98
Surface mobility	629.8	102.9	671.8	191.7
Static feedback on threshold voltage	1.1E-03	9.8E-06	1.1E-01	1.5E-01
Mobility modulation	0.072	0.13	0.09	0.12
Transconductance parameter	6.9E-05	2.3E-05	7.6E-05	2.2E-05
Maximum drift velocity of carriers	2.3E+05	3.4E+05	2.1E+05	1.6E+05
Saturation field factor	0.5	150	0.311	10
Source and drain sheet resistance	0.043	37.95	25.4	3.52
Surface -fast state density	5.2E+11	4.1E+11	5.10E+11	5.10E+11
Type of gate material	1	-1	1	-1
Metallurgical junction depth	3.0E-07	2.0E-07	2.0E-07	2.0E-07
Lateral diffusion	0.0	1.0E-14	1.0E-07	1.1E-08
Gate-drain overlap capacitance per meter	1.7E-10	2.1E-10	1.7E-10	5.0E-11
Gate-source overlap capacitance per meter	1.7E-10	2.1E-10	1.7E-10	5.0E-11
Gate-bulk overlap capacitance per meter	1.0E-10	1.0E-10	5.1E-10	4.3E-10
Zero-bias bulk capacitance per square meter	2.7E-04	3.0E-04	2.8E-04	2.9E-04
Bulk junction potential	0.717	0.737	0.99	0.736
Bulk junction grading coefficient	0.5	0.429	0.526	0.43
Zero-bias perimeter capacitance per meter	1.4E-10	1.6E-10	1.5E-10	1.9E-10

and 3-dB bandwidth were 4.7 (13.44 dB) and 1.06 MHz respectively, which compare reasonably well with the experimental values.

In this chapter, various stages involved in the design of the op-amp are discussed in detail. The simulation and experimental results are presented.

6. DISCUSSIONS, SUMMARY AND FUTURE WORK

6.1 Discussions and Summary

In this work, a system for wireless power transmission is designed to deliver power to a remote location. One potential application is to remotely deliver power to a gastric pacer. Inductive coupling is a convenient method for power transfer from a transmitter coil external to the body to a receiver coil implanted in the body or located remotely. The transmitter coil can be worn around the waist as a belt and the receiver coil will be a part of the implanted system. Both coils form a loosely coupled system.

A 57-turn transmitter coil is wound with a 10 gauge wire size with calculated inductance of 2.5 mH, winding resistance of 0.24 Ω and parasitic capacitance of 47.6 pF. The self-resonance frequency of the transmitter coil is at 462 kHz. A 30-turn receiver coil is wound with a 20 gauge wire size with an inductance of 38.7 μH, winding resistance of 0.146 Ω and parasitic capacitance of 2 pF. The transmitter coil is driven at a resonance frequency of 39.45 kHz which is at least an order of magnitude lower than its self-resonance frequency. The measured values of inductance and the resistance of the transmitter coil at 40 kHz are respectively 2.47 mH and 11.5 Ω. The measured value of the inductance matches well with the calculated value. The measured value of resistance is considerably higher than the calculated value and is attributed to skin effect.

The measured values of inductance and the resistance of the receiver coil at 40 kHz are respectively 38.85 μH and 0.405 Ω. Again, the measured inductance value compares well with the calculated value. The slightly higher value of resistance is attributed to skin effect. The maximum rms supply voltage to drive the transmitter coil at 39.45 kHz was 0.35 V. The values

of the external capacitors used to resonate the transmitter and the receiver coils at operating frequency were 6.7 nF and 0.45 μF respectively.

The induced voltage in the receiver coil is rectified by a full wave rectifier whose output is connected to the load resistor R_L. The load in this application is an IC chip, which is used to recharge Li batteries implanted in the body. This chip requires a dc voltage of 6.5 V and a dc current of 100 mA for its operation. This charging chip is replaced by an equivalent resistance of 65 Ω. The expressions for the load voltage and power are derived. Theoretically, the transmitter coil requires an input rms supply voltage of 0.85 V for the load resistor to meet the requirements if no other losses are present in the circuit. Practically, for an input rms supply voltage of 0.35 V, the rms voltage across the load resistor is 0.37 V when the receiver coil is placed at the center of the transmitter coil. When the receiver coil is moved laterally to the rim of the transmitter coil the observed rms voltage across the load resistor is 0.67 V for the same input supply of 0.35 V. Hence the measured transmitted power to the load of the receiver coil is 4 mW and 13.2 mW when the receiver coil is placed at the center and at the rim of the transmitter coil respectively. These are significantly lower than the calculated values.

The required specifications can be achieved by increasing the input supply voltage. At the input rms supply voltage of 25.7 V, the theoretical value obtained for the voltage induced and the power transmitted to the $R_L/2$ resistor are respectively 4.7 V and 650 mW. The power for an input rms supply voltage of 25.7 V is $25.7^2/11.5 = 57.4\,\text{W}$, assuming that the transmitter coil is at resonance and the effect of reflected impedance of the receiver coil is negligible. The performance of the remote power delivery system can be also improved by matching the resonance frequencies of the transmitter and the receiver coils.

The second objective of this work is to design an operational amplifier (op-amp) for on-chip amplification of sensor signal in a MEMS based microsystem. For example, the differential signal from the LMGFET (lateral moving gate field effect transistor) accelerometer can be amplified by this on-chip op-amp. The differential output voltage of the LMGFET accelerometer to be sensed is in mV range. A minimum of 20 kHz bandwidth is required, since the accelerometer is used to sense the signals in audio frequency range. Op-amp with a gain of 108 (40.7 dB) and 3-dB bandwidth of 580 kHz is designed. Designed op-amp is simulated using PSPICE with Level-3 MOS model parameters. The PSPICE 'net list' was extracted from the physical layout of the amplifier using Tanner L-EDIT 8.20. Experimental measurements observed a gain of 3 and 3-dB bandwidth of 1 MHz. The experimental results did not match with the design simulations. This is attributed to differences in the MOS model parameter values used in the simulations compared to the values appropriate for the process utilized by the foundry. When simulations were redone using the parameter values given by the foundry, the new value for gain and 3-dB bandwidth were 4.7 (13.44 dB) and 1.06 MHz respectively, which compare reasonably well with the experimental values.

6.2 Future Work

Although significant advances have been made during this work, there are several areas in which further investigation would be useful. A few of these areas are discussed in this section.

The power transfer efficiency between the transmitter and the receiver coil can be improved. High power transfer efficiency can be achieved by using a ferrite core material for the receiver coil.

By using a center tapped receiver coil, half wave rectifier can be used for rectification of the signal. Thus, reducing the number of components implanted.

The op-amp has to be redesigned for higher gain.

REFERENCES

1. William J. Heetderks, "RF Powering of Millimeter and Submillimeter-Sized Neural Prosthetic Implants," IEEE Trans. Biomed. Eng., vol. 35, No. 5, pp. 323-327, May 1988.

2. Wen H. Ko, Sheau P. Liang, and Cliff D. F. Fung, "Design of radio-frequency powered coils for implant instruments," Med. & Biol. Eng. & Comput., vol. 15, pp. 634-640, 1977.

3. John C. Schuder, Jerry H. Gold, and Hugh E. Stephenson Jr., "An Inductively Coupled RF System for the Transmission of 1 kW of Power Through the Skin," IEEE Trans. Biomed. Eng., vol. MNE-18, No. 4, pp. 265-273, July 1971.

4. Babak Ziaie, Mark D. Nardin, Anthony R. Coghlan, and Khalil Najafi, "A Single-Channel Implanted Microstimulator for Functional Neuromuscular Stimulator," IEEE Trans. Biomed. Eng., vol. 44, No. 10, pp. 909-920, October 1997.

5. Brian Smith, P. Hunter Peckham, Michael W. Keith, and Dennis D. Roscoe, "An External Powered, Multichannel, Implantable Stimulator for Versatile Control of Paralyzed Muscle," IEEE Trans. Biomed. Eng., vol. BME-34, No. 7, pp. 499-507, July 1987.

6. Mani Soma, Douglas C. Galbraith, and Robert L. White, "Radio-Frequency Coils in Implantable Devices: Misalignment Analysis and Design Procedure," IEEE Trans. Biomed. Eng., vol. BME-34, No. 4, pp. 276-282, April 1987.

7. F. C. Flack, E. D. James, and D. M. Schlapp, "Mutual Inductance of Air-cored Coils: Effect on Design of Radio-frequency Coupled Implants," Med. & biol. Engng. Vol. 9, pp. 79-85, Pergamon Press, January1971.

8. Erwin S. Hochmair, "System Optimization for Improved Accuracy in Transcutaneous Signal and Power Transmission," IEEE Trans. Biomed. Eng., vol. BME-31, No. 2, pp. 177-186, February 1984.

9. Jie Wu, Victor Quinn, and Gary H. Bernstein, "A simple, wireless powering scheme for MEMS devices," Proc. of SPIE Vol. 4559, pp. 43-52, 2001.

10. J. C. Schuder, and H. E. Stephenson, Jr., "Energy Transport to a Coil Which Circumscribes a Ferrite Core and Is Implanted Within the Body," IEEE Trans. Biomed. Eng., vol. BME-12, Nos. 3 and 4, pp. 154-163, July/October 1965.

11. Koenraad Van Schuylenbergh, and Robert Puers, "Self Tuning Inductive Powering for Implantable Telemetric Monitoring Systems," 8th International Conference on Solid-State Sensors and Actuators, and Eurosensors IX, Stockholm, Sweden, pp. 55-58, June 25-29, 1995.

12. R. Puers, M. Catrysse, G. Vandevoorde, R. J. Collier, E. Louridas, F. Burny, M. Donkerwolcke, and F. Moulart, “An Implantable System for Detecting Loosening of a Hip Prosthesis,” in International Symposium on Biotelemetry, Juneau, USA, Program and abstracts, pp. 63-64, May 9-14, 1999.

13. N. de N. Donaldson, and T. A. Perkins, “Analysis of resonant coupled coils in the design of radio frequency transcutaneous links,” Med. Biol. Eng. & Comput, Vol. 21, pp. 612-627, September 1983,

14. Paul R. Gray, and Robert G. Meyer, “MOS Operational Amplifier Design – A Tutorial Overview,” IEEE Journal of solid-state circuits, Vol. SC-17, No. 6, pp. 969-982, December 1982.

15. “Reference Data for Radio Engineers”, Fifth edition, Howard W. Sams & Co. Inc., 1972.

16. Jeffrey A. Von Arx “A Fully Integrated Neuromuscular Stimulation System – FINESS”, Doctoral thesis, University of Michigan, Ann Arbor, 1998.

17. In-hyouk Song, Sunitha Kopparthi, Pratul K. Ajmera and Ashok Srivastava, “Design, Simulation and Fabrication of a Novel Integrated Microaccelerometer Utilizing a Post-CMOS Fabrication technique”, Proc. SPIE Conference on smart structure and materials 2003, Smart Electronics, MEMS, BioMEMS, and Nanotechnology, Vol. 5055, pp. 78-86, March 2003.

18. R. T. Howe, and C. Sodini, “Microelectronics: An Integrated Approach”, Prentice Hall, Upper Saddle River, 1996.

19. Phillip E. Allen, and Douglas R. Holberg, “CMOS Analog Circuit Design”, Oxford University Press, New York Oxford, 2002.

20. Malcolm R. Haskard, and Ian C. May, “Analog VLSI Design nMOS and cMOS,” Prentice Hall, New York, 1988.

21. Yannis Tsividis, “Mixed Analog – Digital VLSI Devices and Technology: An Introduction,” McGraw – Hill Professional, March, 1996.

APPENDIX A: ANNEALED COPPER AND FORM FACTOR DETAILS

Table A.1: Annealed copper --- Comparison of gauges from reference [15].

AWG B & S Gauge	Min diameter of the bare wire in mils	Diameter* in mils	Ft per Lb	Ft per ohm
10	102.4	104.4	31.82	1001
11	91.3	93.2	40.12	794.0
12	81.4	83.2	50.59	629.6
13	72.6	74.3	63.80	499.3
14	64.8	66.4	80.44	396.0
15	57.8	59.3	101.4	314.0
16	51.5	52.9	127.9	249.0
17	46	47.3	161.3	197.5
18	41	42.2	203.4	156.6
19	36.6	37.8	256.5	124.2
20	32.6	33.8	323.4	98.50
21	29.2	30.3	407.8	78.11
22	26.1	27	514.2	61.95
23	23.2	24.2	648.4	49.13
24	20.8	21.6	817.7	38.96
25	18.6	19.3	1031.0	30.90
26	16.6	17.2	1300	24.50
27	14.9	15.5	1639	19.43
28	13.2	13.8	2067	15.41
29	11.9	12.5	2607	12.22
30	10.5	11.1	3287	9.691
31	9.4	9.9	4145	7.685
32	8.5	9	5227	6.095
33	7.5	8	6591	4.833
34	6.7	7.1	8310	3.833
35	5.9	6.3	10480	3.040
36	5.3	5.7	13210	2.411
37	4.7	5.1	16660	1.912
38	4.2	4.6	21010	1.516
39	3.6	4	26500	1.202
40	3.2	3.6	33410	0.9534

* Nominal bare diameter plus maximum additions.

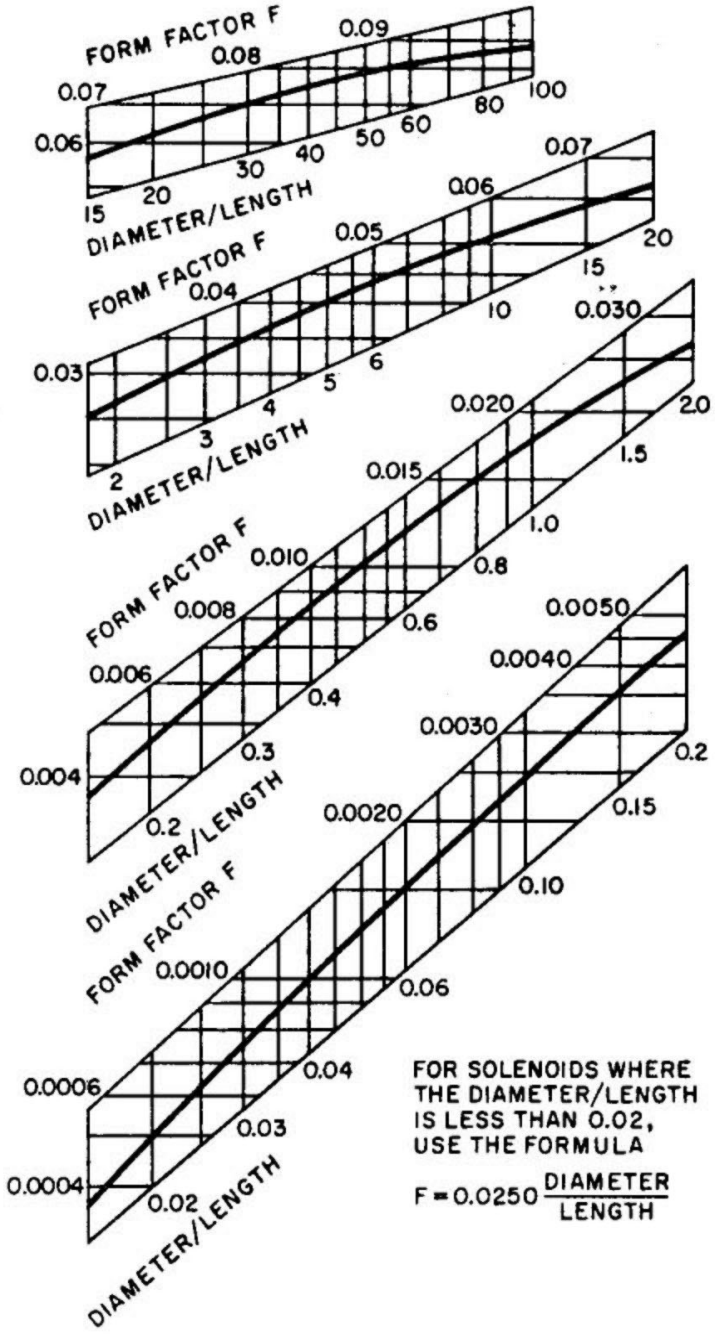

Fig. A.1: Inductance of a single-layer solenoid, form factor = F.
From reference [15].

APPENDIX B: SPICE NETLIST FILE

Netlist for simulating the op-amp shown in Fig. 5.2.

∗ The various nodes are as follows: Node 2 - V_{DD}, Node 8 – non-inverting I/P,

* Node 3- inverting I/P, Node 10 – V_{SS}, Node 4 – second-stage output,

* Node 5 – first-stage output.

* Differential pair

M1 5 8 1 1 PMOS W = 48U L = 6U

M2 7 3 1 1 PMOS W = 48U L = 6U

* NMOS current mirror

M3 7 7 10 10 NMOS W = 30U L = 6U

M4 5 7 10 10 NMOS W = 30U L = 6U

* PMOS current mirror

M5 9 9 2 2 PMOS W = 18U L = 6U

M6 1 9 2 2 PMOS W = 18U L = 6U

* Compensation capacitor

Cc 5 4 6fF

* Second stage

M7 4 5 10 10 NMOS W = 60U L = 6U

M8 4 9 2 2 PMOS W = 60U L = 6U

* Active resistor

M9 10 10 9 2 PMOS W = 18U L = 6U

* Extracted parasitics

Cpar1 1 0 9.79616f

Cpar2 2 0 13.20752f

* Warning: Node 3 has zero nodal parasitic capacitance.

Cpar4 4 0 9.95072f

Cpar5 5 7.60656f

Cpar6 7 6.44f

* Warning: Node 8 has zero nodal parasitic capacitance.

Cpar7 9 07.5504f

Cpar8 10 0 11.56992f

* Total Nodes: 9;

* Total Elements: 17;

* Extract Elapsed Time: 0 seconds;

* *

* * * * * * * Level-3 MOS model parameters * * * * * * * * * *

*

. MODEL NMOS NMOS LEVEL=3 PHI=0.700000 TOX=3.0700E-08 XJ=0.200000U
+ TPG=1 VTO=0.687 DELTA=0.0000E+00 LD=1.0250E-07 KP=7.5564E-05
+ UO=671.8 THETA=9.0430E-02 RSH=2.5430E+01 GAMMA=0.7822
+ NSUB=2.3320E+16 NFS=5.9080E+11 VMAX=2.0730E+05 ETA=1.1260E-01
+ KAPPA=3.1050E-01 CGDO=1.7294E-10 CGSO=1.7294E-10 CGBO=5.1118E-10
+ CJ=2.8188E-04 MJ=5.2633E-01 CJSW=1.4770E-10 MJSW=1.00000E-01
+ PB=9.9000E-01

. MODEL PMOS PMOS LEVEL=3 PHI=0.700000 TOX=3.0700E-08 XJ=0.200000U
+ TPG=-1 VTO=-0.7574 DELTA=2.9770E+00 LD=1.0540E-08 KP=2.1562E-05
+ UO=191.7 THETA=1.2020E-01 RSH=3.5220E+00 GAMMA=0.4099
+ NSUB=6.4040E+15 NFS=5.9090E+11 VMAX=1.6200E+05 ETA=1.4820E-01
+ KAPPA=1.0000E+01 CGDO=5.0000E-11 CGSO=5.0000E-11 CGBO=4.2580E-10
CJ=2.9596E-04 MJ=4.2988E-01 CJSW=1.8679E-10 MJSW=1.5252E-01
+ PB=7.3574E-01

Vdd 2 0 dc 5V

Vss 10 0 dc 0V

VIN1 8 0 SIN (0 6mV 1000)

VIN2 3 0 SIN (0 6mv 1000 0 0 180)

. TRAN 0.1us 2ms

* VIN1 8 0 DC 0V

* VIN2 3 0 AC 48mV

*. AC DEC 20 100 5e8

. OP

. PROBE

. END

VITA

Sunitha Kopparthi was born in 1978 in the Andhra Pradesh, southern state of India. She finished her bachelor of engineering degree in electrical and communication engineering at Andhra University, India, in 2000. She is currently a candidate for the degree of Master of Science in Electrical and Computer Engineering at Louisiana State University.